uc3m | Universidad Carlos III de Madrid

e-Archivo

This is a postprint version of the following published document:

Jacobsen, J. L. & Salas, J. (2006). Transfer Matrices and Partition-Function Zeros for Antiferromagnetic Potts Models IV. Chromatic Polynomial with Cyclic Boundary Conditions. *Journal of Statistical Physics, 122*(4), pp. 705–760.

DOI: 10.1007/s10955-005-8077-8

© 2006, Springer Science Business Media, Inc.

Transfer Matrices and Partition-Function Zeros for Antiferromagnetic Potts Models

IV. Chromatic polynomial with cyclic boundary conditions

Jesper Lykke Jacobsen
Laboratoire de Physique Théorique et Modèles Statistiques
Université Paris-Sud
Bâtiment 100
F-91405 Orsay, FRANCE
JACOBSEN@IPNO.IN2P3.FR

Jesús Salas
Grupo de Modelización, Simulación Numérica y Matemática Industrial
Universidad Carlos III de Madrid
Avda. de la Universidad, 30
28911 Leganés, SPAIN
JSALAS@MATH.UC3M.ES

July 16, 2004
Revised: January 18, 2005
Final version: August 25, 2005

Abstract

We study the chromatic polynomial $P_G(q)$ for $m \times n$ square- and triangular-lattice strips of widths $2 \leq m \leq 8$ with cyclic boundary conditions. This polynomial gives the zero-temperature limit of the partition function for the antiferromagnetic q-state Potts model defined on the lattice G. We show how to construct the transfer matrix in the Fortuin–Kasteleyn representation for such lattices and obtain the accumulation sets of chromatic zeros in the complex q-plane in the limit $n \to \infty$. We find that the different phases that appear in this model can be characterized by a topological parameter. We also compute the bulk and surface free energies and the central charge.

Key Words: Chromatic polynomial; antiferromagnetic Potts model; triangular lattice; square lattice; transfer matrix; Fortuin–Kasteleyn representation; Beraha numbers; conformal field theory.

1 Introduction

The two-dimensional Potts model conceals a very rich physics, in particular in the antiferromagnetic regime. Let $G = (V, E)$ be a finite undirected graph with vertex set V and edge set E. The q-state Potts model is initially defined for q a positive integer in terms of spins $\sigma_x = 1, 2, \ldots, q$ living on the vertices $x \in V$. Its Hamiltonian reads

$$H(\{\sigma\}) \;=\; -J \sum_{\langle xy \rangle \in E} \delta(\sigma_x, \sigma_y) \;, \tag{1.1}$$

where δ is the Kronecker delta. Fortuin and Kasteleyn [1] have shown that the partition function at inverse temperature β can be rewritten as

$$Z_G(q, v) \;=\; \sum_{E' \subseteq E} q^{k(E')} v^{|E'|} \;, \tag{1.2}$$

with $v = \mathrm{e}^{\beta J} - 1$. The sum runs over the $2^{|E|}$ subsets $E' \subseteq E$, with $k(E')$ being the number of connected components (including isolated vertices) in the subgraph (V, E'). We now promote (1.2) to the definition of the model, which permits us to consider q as an arbitrary complex number.

We shall here be interested in the zero-temperature antiferromagnetic case $J = -\infty$ (i.e., $v = -1$), whose restriction to q a positive integer can be interpreted as a coloring problem. In this case, $P_G(q) \equiv Z_G(q, -1)$ is known as the chromatic polynomial. Its evaluation for a general graph is a hard problem in the sense that the best algorithms currently available have a worst-case execution time which grows exponentially with the number of sites of the graph. For strip graphs (or, more generally, recursive families of graphs) the chromatic polynomial $P_{G_n}(q)$ of any member of the family G_n can be computed from a transfer matrix T and certain boundary condition vectors $\boldsymbol{u}$ and $\boldsymbol{v}$:

$$P_{G_n} \;=\; \boldsymbol{u}^T \cdot \mathsf{T}^n \cdot \boldsymbol{v} \;. \tag{1.3}$$

Thus, the computation time grows as a polynomial in n; it does however still grow exponentially in the strip width (due to the L dependence of $\dim \mathsf{T}$). Thus, it is necessary to introduce new algorithms to be able to handle as large L as possible. For example, identifying symmetries may give an equivalent transfer matrix of lower dimension (in this respect, the Fortuin-Kasteleyn representation makes manifest the S_q symmetry of the original spin Hamiltonian).

It is important to remark that the Potts spin model has a probabilistic interpretation (i.e., has non-negative Boltzmann weights) only when q is a positive integer and $v \geq -1$. The Fortuin–Kasteleyn random-cluster model (1.2), which extends the Potts model to non-integer q, has non-negative weights only when $q \geq 0$ and $v \geq 0$. In all other cases, the model belongs to the "unphysical" regime (i.e., some weights are negative or complex), and some familiar properties of statistical mechanics need not hold. For example, even for integer $q \geq 2$ and real v in the range $-1 \leq v < 0$, where the *spin* representation exists and has non-negative weights, the dominant eigenvalue λ_1 of the transfer matrix in the *cluster* representation need not be simple (i.e., the eigenvector may not be unique); and even if simple, it may not play any role in determining $Z_{G_n}(q, v)$ because the corresponding amplitude may vanish.

Both these behaviors are of course impossible for any transfer matrix with *positive* weights, by virtue of the Perron–Frobenius theorem. It is important to note that the dominant eigenvalues in the cluster and spin representations need not to be equal, because one of them may have a vanishing amplitude (see below). In any case, the Potts model can thus make probabilistic sense in the cluster representation at parameter values where it fails to make probabilistic sense in the spin representation, and vice versa. It is worth mentioning that for $q = 4\cos^2(\pi/n)$ with integer $n = 3, 4, \ldots$ and *planar* graphs G, the Potts-model partition function $Z_G(q, v)$ admits a third representation, in terms of a restricted solid-on-solid (RSOS) model [2, 3].

But even in the most general case (i.e., with arbitrary real, or even complex q and v) we consider the study of the random-cluster model (1.2) fully legitimate. Note in this context that there is a long story of studying statistical-mechanical models in "unphysical" regimes (e.g., the hard-core lattice gas at its negative-fugacity critical point [4, 5, 6, 7, 8, 9, 10, 11, 12, 13] or the Yang–Lee edge singularity [14, 15, 16, 17, 18, 19, 20]). In particular, Baxter [21] studied the zero-temperature limit of the triangular-lattice Potts antiferromagnet, which belongs to this "unphysical" regime. Generally speaking, the "unphysical" regime can be understood using the standard tools of statistical mechanics with appropriate modifications. In particular, although a rigorous proof is still lacking, conformal field theory (CFT) seems to apply also in the "unphysical" regions (see e.g., [19, 20] for the CFT description of the Lee-Yand edge singularity). In general, "unphysical" regions are described by non-unitary field theories.

It is well established that antiferromagnetic models in general, and the chromatic polynomial in particular, are very sensitive to the choice of boundary conditions. Indeed, different choices may lead to quite different thermodynamic limits. Following our earlier publications [22, 23, 24], where we studied free or periodic boundary conditions in the transverse (space-like) direction and *free* boundary conditions in the longitudinal (time-like) direction, we here subject the chromatic polynomial to *cyclic boundary conditions*, i.e., free in the transverse direction and *periodic* in the longitudinal direction. For a transfer matrix written in the Potts spin basis, cyclic boundary conditions can be easily implemented by setting $P_{G_n} = \mathrm{Tr}\,\mathsf{T}^n$. The situation is, however, less straightforward in the Fortuin–Kasteleyn representation, and we are obliged to employ a transfer matrix that is different from —and more complicated than— the ones used in [22, 23, 24].

Our study is of interest for understanding the general properties of the so-called Berker-Kadanoff (BK) phase in the antiferromagnetic Potts model [26]. Generically, the *two-dimensional* Potts model on a given regular lattice possesses a curve $v_{\mathrm{FM}}(q) > 0$ of ferromagnetic phase transitions which are second-order in the range $0 < q \leq 4$ [27]. Along this curve the thermal operator (which corresponds to taking v away from its critical value $v_{\mathrm{FM}}(q)$) is relevant and it becomes marginal in the limit $q \to 0$ of spanning trees. The analytic continuation of the curve $v_{\mathrm{FM}}(q)$ into the antiferromagnetic regime yields a second critical curve $v_{\mathrm{BK}}(q) < 0$ with $0 < q < 4$ along which the thermal operator is *irrelevant*. Therefore, for each $q \in (0, 4)$, the critical point $v_{\mathrm{BK}}(q)$ acts as the renormalization-group attractor of a finite range of v values: this is the BK phase.

The above scenario has been verified in detail for several regular lattices. In particular, for the square and triangular lattices the corresponding models are Bethe Ansatz soluble

[28][1] and the analytic forms of $v_{\rm FM}(q)$ and $v_{\rm BK}(q)$ are exactly known. The scenario is also inherent in the Coulomb gas approach to critical phenomena [29], which, albeit less rigorous, confirms that the general properties of the BK phase are lattice independent.

The best understood case is that of the square lattice. Here, $v_{\rm FM}(q) = +\sqrt{q}$ and $v_{\rm BK}(q) = -\sqrt{q}$ [28, 26]. There are also two mutually dual (and hence equivalent) curves of antiferromagnetic transition points [30], $v_\pm(q) = -2 \pm \sqrt{4-q}$ for $q \in [0,4]$, which are believed to form the boundaries of the BK phase [26]. Exactly on $v_\pm(q)$, the model exhibits a different type of critical behavior [26, 31].

More precisely, for a given width L and $q \in I(L)$ belonging to a suitable interval $I(L)$, there exists mutually dual couplings $v_\pm(q,L)$ so that for $v_-(q,L) < v < v_+(q,L)$, the dominant eigenvalue $\lambda_{\rm BK}(v)$ in the cluster representation is simple. As $L \to \infty$, one has $v_\pm(q,L) \to v_\pm(q)$ and $\lim_{L\to\infty} I(L)$ contains $[0,4]$. The finite-size scaling of $\lambda_{\rm BK}(v)$, and of its adjacent scaling levels, determines the critical exponents of the BK phase. However, for certain special values of q (the generalized Beraha numbers, see below) the amplitudes of $\lambda_{\rm BK}(v)$, and of many subdominant eigenvalues, vanish; yet other eigenvalues are degenerate in pairs but have amplitudes of opposite sign and thus, cancel out from the partition function. The remaining eigenvalues correspond to those of the relevant RSOS representation (or spin representation, when q is a positive integer). On the other hand, for $v \notin [v_-(q,L), v_+(q,L)]$ the dominant eigenvalue in the cluster representation is again simple, but is a *different* analytical expression of v, and its amplitude does *not* vanish at the special values of q.

On the triangular lattice, $v_{\rm FM}(q)$ is the uppermost branch ($v > 0$) of the curve $v^3 + 3v^2 - q = 0$ [32]. We know of numerical evidence (to be published elsewhere) that the middle and lower branches of this same curve may be respectively $v_{\rm BK}(q)$ and the lower boundary $v_-(q)$ of the BK phase. Less is known about the upper boundary $v_+(q)$ of the BK phase. If we assume, in analogy with the square-lattice case, that it is the first locus of partition function zeros encountered in the antiferromagnetic regime upon decreasing the temperature from infinity, one has $v_+(0) = 0$, and the slope $\frac{\rm d}{{\rm d}q} v_+(q)\Big|_{q\to 0^+} \simeq -0.1753 \pm 0.0002$ is known numerically [33]. Moreover, another Bethe Ansatz soluble case [21], $v = -1$, provides evidence that $v_+(q_0) = -1$, where q_0 will be defined below.

In the present publication we study the chromatic polynomial with cyclic boundary conditions for the square and the triangular lattices. In both cases the chromatic line $v = -1$ passes through a finite part of the BK phase, whence our results will enable us to examine the role of cyclic boundary conditions for this phase. We shall obtain strong evidence that with cyclic boundary conditions the BK phase splits into an *infinite number of distinct phases*, each of which has a precise topological characterization in terms of the Fortuin-Kasteleyn clusters. However, the chromatic line only intersects a finite number of these phases. For the square (resp. triangular) lattice chromatic polynomial we thus find a total of three (resp. seven) phases.

In particular, we examine the loci of zeros of $P_{G_{L\times n}}(q)$, for strips of width L and length n,

[1] Baxter [28, 30] has shown that the two-dimensional Potts model is equivalent to a homogeneous six-vertex model on certain curves of the (q,v) plane, including $v_{\rm FM}(q)$ and $v_{\rm BK}(q)$ for both the square and triangular lattices. This homogeneous six-vertex model is soluble using the Bethe Ansatz [28]. In addition, Baxter also showed that the square-lattice model on the mutually dual curves $v_\pm(q)$ is equivalent to a certain class of inhomogeneous six-vertex models that can nevertheless be solved by an extension of the Bethe Ansatz [30].

in the plane of complex q. When $n \to \infty$, the accumulation points of these zeros form either isolated limiting points (when the amplitude of the dominant eigenvalue vanishes) or continuous limiting curves $\mathcal{B}_L$ (when two or more dominant eigenvalues become equimodular). These latter curves constitute the boundaries between the different phases just described. We refer to [22, 23, 24] for details, and for the relation to the Beraha–Kahane–Weiss theorem [34]. The rather unusual phase diagram referred to above is linked to a difference of the $L \to \infty$ limits of $\mathcal{B}_L$ with free/cylindrical [22, 23, 24] and cyclic boundary conditions (this work).

The curves $\mathcal{B}_L$ will in general intersect the real q-axis in a number of values, and we define $q_0(L)$ to be the largest of these values. Also, let $q_0 = \lim_{L\to\infty} q_0(L)$. Based on our earlier studies [22, 23, 24] we expect q_0 for a given lattice to be independent of (reasonable) boundary conditions. The physical scenario outlined above would then imply that we should observe the BK phase for $0 < q < q_0(L)$. We expect $q_0(\mathrm{sq}) = 3$ for the square lattice (corresponding to $v_+(3) = -1$). For the triangular lattice, Baxter [21] originally predicted $q_0(\mathrm{tri}) \approx 3.81967$. We have recently revisited the analysis of Baxter's equations [24], arguing in particular that his prediction for $q_0(\mathrm{tri})$ is erroneous, the correct value being $q_0(\mathrm{tri}) = 2 + \sqrt{3} \approx 3.73205$.

The results available in the literature concerning square- and triangular-lattice strips with cyclic boundary conditions are limited to widths $L \leq 5$. The results for the square lattice were obtained for $L = 2$ by Biggs, Demerell and Sands [35], for $L = 3$ by Shrock and Tsai [36], and for $L = 4, 5$ by Chang and Shrock [37, 38]. The results for the triangular lattice were obtained for $L = 2$ by Shrock and Tsai [36], and for $L = 3, 4$ by Chang and Shrock [39]. When writing up this paper we learned that Chang and Shrock have extended their results to the case $L = 5$ [41].

In this paper we present new exact results for the chromatic polynomial of strip graphs of widths $L = 6$. We have also computed independently the exact formula for the triangular-lattice strip graphs of width $L = 5$; furthermore, we present the computation of the limiting curve for these strips.[2] For $L = 7, 8$ we have *exactly* computed some blocks of the transfer matrix from which *all* the eigenvalues can be inferred (modulo some conjectures that are very plausible though unproven, see Properties 1 and 3 in Section 2.3). Unfortunately some of these blocks are so large than we have been unable to get the analytical expressions for the eigenvalues, as we have done for $L \leq 6$. From the *exact symbolic* expression for these blocks, we can nevertheless obtain *essentially-exact* relevant physical information, such as numerical values for the eigenvalues and the limiting curve $\mathcal{B}$. The only source of error in these results is the limited (but very high) machine precision of the numerical computations performed with MATHEMATICA. We have taken the symbolic computations reported in this paper as far as possible, using several months of CPU time. However, because of the exponential character (in the width L) of this problem, going beyond $L = 8$ will require an extremely large amount of CPU time and RAM memory.

Our approach is based on a transfer-matrix formulation of the Fortuin–Kasteleyn representation, which is equivalent to the methods of Shrock and collaborators (See e.g. [40] and references therein).[3] Large parts of our analysis has been automatized and carried out by

[2] The interested reader can find the exact expression of the eigenvalues for $L \leq 6$ in the MATHEMATICA files available as part of the electronic version of this paper in the `cond-mat` archive.

[3] The two approaches are however formulated in somewhat different terms, so the equivalence is only made clear by a detailed comparison.

a computer, thus allowing to access larger widths L. On the other hand, in our approach we find a natural candidate for an essentially "conserved quantum number": the number of bridges[4] of a given connectivity state (see Section 2.2 for details). This number is the link to the quantum-group theory worked out by Pasquier and Saleur [25, 26]. Finally, let us mention a different approach developed by Noy and Ribó [42] and also based on a transfer-matrix formalism. They handle cyclic boundary conditions by introducing a new type of operation: edge deletion.

The outline of the paper is as follows. In Section 2 we present our method for obtaining the transfer matrix for a square-lattice strip with cyclic boundary conditions. We describe the structural properties of the transfer matrix and its block structure. Section 2.3 also provides an alternative (and simplified) method for constructing the transfer matrix which has proved very useful for large-width computations. In Section 3 we present the results for square-lattice strips up to widths $L = 8$. In the following Section we adopt our method to triangular-lattice strips with cyclic boundary conditions, and the results are given in Section 5 for widths up to $L = 8$. Finally, in Section 6 we discuss the phase diagram of the square- and triangular-lattice Potts antiferromagnet at zero temperature. We compute the free energy and the central charge as a function of q. Finally, in Appendix A we show an alternative way of computing the transfer matrix for a cyclic square-lattice strip.

2 Transfer matrix for square-lattice strips with cyclic boundary conditions

We want to build the transfer matrix for a square-lattice strip of width m and arbitrary length n with cyclic boundary conditions, i.e., free along the transverse direction and periodic along the longitudinal direction (Figure 1 shows an example of size 4×2). As in previous work [22, 23, 24], we would like to express the transfer matrix T as a product of two matrices H and V, representing respectively the horizontal and vertical bonds of the lattice

$$\mathsf{T}(m) \;=\; \mathsf{V}(m) \cdot \mathsf{H}(m) \tag{2.1}$$

For each lattice strip width m we have a different transfer matrix. When free boundary conditions are used in the longitudinal direction (i.e., for a strip with free or cylindrical b.c.), the transfer matrix in the Fortuin–Kasteleyn representation has been explained in detail in [22, Section 3]. The basic idea is that the state of the system is characterized by a connectivity pattern $\{\mathbf{v}_{\mathcal{P}}\}$ of the sites $\{1, \ldots, m\}$ of the top row, and the transfer matrix $\mathsf{T}(m)$ acts by attaching one new row above the current top row.

By contrast, when periodic boundary conditions are used in the longitudinal direction, it is insufficient to keep track of the connectivity of the top row alone, as we will eventually need to identify the top and bottom rows. Rather, as first sketched in [22, Section 7.4], the idea is to keep track of the connectivity pattern of the $2m$ sites constituted by the current top row *and* the bottom row. Let us call these sites $1, 2, \ldots, m$ and $1', 2', \ldots, m'$, respectively (see Figure 1 for an example with $m = 4$). Initially the top and bottom rows are identical. We then enlarge the lattice by adding successive new rows to the top of the lattice, exactly as

[4] The number of bridges is equivalent to what Refs. [41, 40] call the level.

in [22, Section 3.2]; the join and detach operations act on the sites of the top row, with those of the bottom row simply "going along for the ride". At the end, when we have obtained a lattice with $n+1$ rows, we identify the top and bottom rows.

Let us now explain this formalism in greater detail. We characterize the state of the top and bottom rows by a connectivity pattern $\{\mathbf{v}_{\mathcal{P}}\}$, which is associated to a partition $\mathcal{P} = \{P_1, \ldots, P_k\}$ of the set $\{1, \ldots, m, 1', \ldots, m'\}$. It is convenient to introduce the operators

$$\mathsf{P}_x \;=\; vI \,+\, \mathsf{D}_x \tag{2.2}$$

$$\mathsf{Q}_{x,y} \;=\; I \,+\, v\mathsf{J}_{xy} \tag{2.3}$$

acting on $\{\boldsymbol{v}_{\mathcal{P}}\}$ (see [22] for more details). Here, I is the identity; D_x is a detach operator that detaches site x from the block it currently belongs to, multiplying by a factor q if x is currently a singleton; and J_{xy} is a join operator that amalgamates the blocks containing x and y, if they were not already in the same block.

The matrices $\mathsf{H}(m)$ and $\mathsf{V}(m)$ then act on the top row as follows:

$$\mathsf{H}(m) \;=\; \prod_{i=1}^{m-1} \mathsf{Q}_{i,i+1} \tag{2.4a}$$

$$\mathsf{V}(m) \;=\; \prod_{i=1}^{m} \mathsf{P}_i \tag{2.4b}$$

We can similarly define matrices $\mathsf{H}'(m)$ and $\mathsf{V}'(m)$ that act on the bottom row.

The chromatic polynomial of a square-lattice strip of width m and length n with cyclic boundary conditions is given by

$$P_{m\times n}(q) \;=\; \boldsymbol{u}^{\mathrm{T}} \cdot \mathsf{H}(m) \cdot \mathsf{T}(m)^n \cdot \boldsymbol{v}_{\mathrm{id}} \tag{2.5}$$

The left $\boldsymbol{u}$ and right $\boldsymbol{v}_{\mathrm{id}}$ vectors differ from those found for free and cylindrical boundary conditions. The right vector $\boldsymbol{v}_{\mathrm{id}}$ now denotes the partition

$$\boldsymbol{v}_{\mathrm{id}} \;=\; \{\{1,1'\},\{2,2'\},\ldots,\{m,m'\}\} \tag{2.6}$$

(i.e., we start with the top and bottom rims identified). The left vector in (2.5) acts on a connectivity state $\boldsymbol{v}_{\mathcal{P}}$ as follows

$$\boldsymbol{u}^{\mathrm{T}} \cdot \boldsymbol{v}_{\mathcal{P}} \;=\; q^{|\mathcal{P}'|} \tag{2.7}$$

where $|\mathcal{P}'|$ denotes the number of blocks in the connectivity $\boldsymbol{v}_{\mathcal{P}'}$ obtained from $\boldsymbol{v}_{\mathcal{P}}$ by the action of several join operators $\mathsf{J}_{x,y}$:

$$\boldsymbol{v}_{\mathcal{P}'} \;=\; \left(\prod_{i=1}^{m} \mathsf{J}_{i,i'}\right) \cdot \boldsymbol{v}_{\mathcal{P}} \tag{2.8}$$

In other words, $\boldsymbol{u}^{\mathrm{T}}$ acts on $\boldsymbol{v}_{\mathcal{P}}$ by identifying the top and bottom rows, assigning a factor of q to each block in the resulting partition.

In this paper we are mainly concerned by the chromatic-polynomial case ($v = -1$). In this case, the matrix H is a projector (i.e., $\mathsf{H}^2 = \mathsf{H}$). Thus, we can use instead of the transfer matrix T [c.f., (2.1)] and the usual connectivity states $\boldsymbol{v}_{\mathcal{P}}$, the modified transfer matrix

$$\widetilde{\mathsf{T}}(m) \;=\; \mathsf{H}(m) \cdot \mathsf{V}(m) \cdot \mathsf{H}(m) \tag{2.9}$$

and the basis vectors

$$\boldsymbol{w}_{\mathcal{P}} \;=\; \mathsf{H}(m) \cdot \boldsymbol{v}_{\mathcal{P}} \tag{2.10}$$

Note that $\boldsymbol{w}_{\mathcal{P}} = 0$ if $\mathcal{P}$ has any pair of nearest neighbors of the top row in the same block. As we start with the state $\boldsymbol{w}_{\mathrm{id}}$, and at the end we are identifying the top and bottom rows, it is useful to work directly on the modified connectivity basis

$$\widehat{\boldsymbol{w}}_{\mathcal{P}} \;=\; \mathsf{H}'(m) \cdot \mathsf{H}(m) \cdot \boldsymbol{v}_{\mathcal{P}} \tag{2.11}$$

This choice implies that $\widehat{\boldsymbol{w}}_{\mathcal{P}} = 0$ also if $\mathcal{P}$ contains any pair of nearest neighbors of the bottom row in the same block. For simplicity, we hereafter drop the tilde to denote the modified transfer matrix (2.9), and the hat to denote the modified connectivity basis (2.11). In this case, the chromatic polynomial can be written as

$$P_{m\times n}(q) \;=\; \boldsymbol{u}^{\mathrm{T}} \cdot \mathsf{T}(m)^n \cdot \boldsymbol{w}_{\mathrm{id}} \tag{2.12}$$

2.1 Structural properties of the chromatic polynomial

The first observation is that the square lattice with cyclic boundary conditions is a *planar* graph: thus, only non–crossing partitions $\mathcal{P}$ of $\{1,\ldots,m,1',\ldots,m'\}$ can occur. As we have transverse free boundary conditions, the number of such connectivities is given by the Catalan number

$$C_{2m} \;=\; \frac{1}{2m+1}\binom{4m}{2m} \tag{2.13}$$

Their asymptotic behavior is given by

$$C_{2m} \;=\; 16^m m^{-3/2}(8\pi)^{-1/2}[1+O(1/m)] \tag{2.14}$$

These numbers are listed in the second column of Table 1 up to $m = 10$.

The fact that we are computing the chromatic polynomial ($v = -1$) implies that the dimension of the transfer matrix should be equal to the number of non-crossing *non-nearest-neighbor* partitions (i.e., partitions in which no block contains a pair of nearest neighbors). We shall denote these numbers by TriRing(m), as we expect them to be equal to the dimension of T for a cyclic triangular-lattice strip of width m (see Table 1).

A further simplification comes from considering classes of partitions invariant under reflections with respect to the center of the strip. The number of such invariant classes is denoted by SqRing(m) in Table 1. Thus, we expect that these numbers are equal to the dimension of T for a cyclic square-lattice strip of width m.

We have modified the `perl` code that we used for free/cylindrical boundary conditions [23, 24] to deal with the cyclic boundary conditions. We have found that for $m \geq 3$, SqRing(m) is larger than the number of *distinct* eigenvalues SqRing$'(m)$ found in [36, 37, 43] (see Table 1).[5] In Section 2.3 below we show how the transfer matrix can be rewritten in a form that amounts to making each distinct eigenvalue appear with unit multiplicity; we also explain how the issue of degeneracies is linked to an underlying quantum-group symmetry.

[5]The authors of Ref. [43] use the notation $N_{P,L_y,\lambda}$ to denote the number of distinct eigenvalues appearing in the chromatic polynomial for cyclic strips of square and triangular lattices of width L_y.

Chang and Shrock found a closed expression for the numbers $\mathrm{SqRing}'(m)$ using coloring-matrix methods [43]:

$$\mathrm{SqRing}'(m) \;=\; 2(m-1)! \sum_{k=0}^{\lfloor m/2 \rfloor} \frac{(m-k)!}{(k!)^2\,(m-2k)!} \tag{2.15}$$

We notice that these numbers coincide with the sequence `A025565` of [44], and we therefore have the alternative expression[6]

$$\mathrm{SqRing}'(m) \;=\; \sum_{k=0}^{\lfloor (m+1)/2 \rfloor} \binom{m-1}{k} \binom{m+1-k}{k+1} . \tag{2.16}$$

The asymptotic behavior for large m of the number of distinct eigenvalues was found by Chang and Shrock [43] to be

$$\mathrm{SqRing}'(m) \;\sim\; 3^m\, m^{-1/2} \qquad \text{as } m \to \infty \tag{2.17}$$

Remarks: 1) This transfer matrix is not invariant under the interchange of the top and bottom rows (i.e. $i \leftrightarrow i'$). The reason is that our transfer matrix only acts on the top row, leaving fixed the bottom one. Thus, we cannot reduce the size of the transfer matrix by including only connectivity states that are invariant under the transformation $i \leftrightarrow i'$.

2) With our transfer-matrix approach we have checked all previous results by Shrock and collaborators [36, 37, 39, 38].

3) Even though the final dimension of the transfer matrix $\mathsf{T}(m)$ is given by $\mathrm{SqRing}(m)$, the computations need to be performed in the larger space of non-crossing connectivities (of dimension C_{2m}). This fact limits the maximum width we are able to handle.

4) When we apply the operator $\prod_{i=1}^{m} \mathsf{J}_{i,i'}$ to a non-crossing connectivity $\boldsymbol{v}_{\mathcal{P}}$ in (2.8), the resulting connectivity state $\boldsymbol{v}_{\mathcal{P}'}$ is *not* guaranteed to be non-crossing. However, as this step is the last one in the computation, we do not need to enlarge our vector space (to include all crossing connectivities).

5) We have checked our results by comparing them to the appropriate chromatic polynomial with cylindrical boundary conditions

$$Z_{m_{\mathrm{F}} \times n_{\mathrm{P}}}(q) = Z_{n_{\mathrm{P}} \times m_{\mathrm{F}}}(q) \;, \tag{2.18}$$

where F and P denote free and periodic boundary conditions respectively.

[6] The equivalence between (2.15) and (2.16) comes from the equality of their respective generating functions. In particular [43],

$$\sqrt{\frac{1+x}{1-3x}} - 1 \;=\; \sum_{m=1}^{\infty} \mathrm{SqRing}'(m)\, x^m$$

2.2 Block structure of the transfer matrix

The transfer matrix for a cyclic square-lattice strip of width m has a block structure. This property greatly simplifies the computation of its eigenvalues as we shall see below. Given a certain connectivity $\mathcal{P}$ of the top and bottom rows (see, e.g., Figure 2), one can regard it as a top-row connectivity $\mathcal{P}_{\rm top}$ and a bottom-row connectivity $\mathcal{P}_{\rm bottom}$ joined by ℓ bridges. Note that each top-row block is connected by at most one bridge to the bottom row and vice versa. Thus, ℓ can take any integer value from 0 to m.

In order to obtain the matrix element $\mathsf{T}_{\boldsymbol{a},\boldsymbol{b}}$ between two connectivity states $\boldsymbol{w}_{\mathcal{P}}$ and $\boldsymbol{w}_{\mathcal{P}'}$, we should perform three operations

1. Apply the vertical-bond operator V on the initial state $\boldsymbol{w}_{\mathcal{P}}$.
2. Apply the horizontal-bond operator H, so we kill any nearest-neighbor connectivity state.
3. Project the result onto the final state $\boldsymbol{w}_{\mathcal{P}'}$.

Let us suppose we start from a connectivity state $\boldsymbol{w}_{\mathcal{P}}$ with a certain bottom-row connectivity $\mathcal{P}_{\rm bottom}$, number of bridges ℓ, and position of such bridges (all these characteristics modulo reflections with respect to the center of the strip). Then two important observations should be made:

- The bottom-row connectivity of the initial state is not modified by the application of either matrix V (in step 1) or matrix H (in step 2).
- The application of the matrices V (in step 1) and H (in step 2) cannot increase the number of bridges ℓ. Thus, we can only go to connectivity states $\mathcal{P}'$ with the same or smaller number of bridges $\ell' \le \ell$. Indeed, the relative position of the bridges is preserved.

These two properties imply that the transfer matrix has a lower-triangular block form:

$$\mathsf{T}(m) \;=\; \begin{pmatrix} T_{m,m} & 0 & \ldots & 0 \\ T_{m-1,m} & T_{m-1,m-1} & \ldots & 0 \\ \vdots & \vdots & & \vdots \\ T_{0,m} & T_{0,m-1} & \ldots & T_{0,0} \end{pmatrix} \tag{2.19}$$

(Note that we have arranged the connectivity states according to a decreasing number of bridges.) Furthermore, they also imply that each diagonal block $T_{\ell,\ell}$ has a diagonal-block form

$$T_{\ell,\ell} \;=\; \begin{pmatrix} T_{\ell,\ell,1} & 0 & \ldots & 0 \\ 0 & T_{\ell,\ell,2} & \ldots & 0 \\ \vdots & \vdots & & \vdots \\ 0 & 0 & \ldots & T_{\ell,\ell,N_\ell} \end{pmatrix} \tag{2.20}$$

where each sub-block $T_{\ell,\ell,j}$ is characterized by a certain bottom-row connectivity $\mathcal{P}_{\rm bottom}$ and a position of the ℓ bridges. Its dimension is given by the number of top-row connectivities

that are compatible with $\mathcal{P}_{\rm bottom}$, ℓ, and the relative positions of the ℓ bridges. The number of blocks N_ℓ ($0 \le \ell \le m$) for a square-lattice strip of width m is displayed in Table 2.

In particular, this structure means that the characteristic polynomial of the full transfer matrix T can be factorized as follows

$$\chi(\mathsf{T}) \;=\; \prod_{\ell=0}^{m} \left[\prod_{j=1}^{N_\ell} \chi\left(T_{\ell,\ell,j}\right) \right] \tag{2.21}$$

In practice, for each strip width $2 \le m \le 6$, we have performed the following procedure:

1. Using a `perl` script, we compute the full transfer matrix $\mathsf{T}(m)$ and the left $\boldsymbol{u}$ and right vectors $\boldsymbol{w}_{\rm id}$. These objects are obtained in the basis of non-crossing non-nearest-neighbor classes of connectivities that are invariant under reflections (with respect to the center of the strip). Thus, their dimension is given by SqRing(m).

2. Given the full transfer matrix $\mathsf{T}(m)$, we compute the SqRing$'(m)$ distinct eigenvalues $\lambda_i(q)$. To do this, we split the transfer matrix into blocks $T_{\ell,\ell,j}$, each block characterized by a bottom-row connectivity and the number ℓ and position of the bridges (modulo reflections). By diagonalizing these blocks we obtain the SqRing$'(m)$ distinct eigenvalues $\lambda_i(q)$ and their multiplicities k_i.[7] Indeed,

$$\sum_{i=1}^{\mathrm{SqRing}'(m)} k_i \;=\; \mathrm{SqRing}(m) \tag{2.22}$$

3. The final goal is to express the chromatic polynomial in the form

$$P_{m\times n}(q) \;=\; \sum_{i=1}^{\mathrm{SqRing}'(m)} \alpha_i(q)\, \lambda_i(q)^n \tag{2.23}$$

   where the $\{\lambda_i\}$ are the distinct eigenvalues of the transfer matrix $\mathsf{T}(m)$ and the $\{\alpha_i\}$ are some amplitudes we have to determine. The calculation of the amplitudes can be achieved by solving SqRing$'(m)$ linear equations of the type (2.23), where the l.h.s. (i.e., the true chromatic polynomials) have been obtained via Eq. (2.12) (i.e., by using the full transfer matrix and vectors).

We have used this procedure to compute the transfer matrix up to width $m = 6$. The next case would involve the calculation of a symbolic matrix of dimension SqRing$(m = 7) = 28940$, which is unmanageable given our computer facilities.

Remark. In the procedure described above one can obtain the eigenvalues $\lambda_i(q)$ of the transfer matrix by considering the diagonal blocks $T_{\ell,\ell}$ [c.f., (2.19)]. However, we still need the full transfer matrix in order to determine the amplitudes $\alpha_i(q)$.

[7] Unfortunately, we have not found any analytical formula for the multiplicities k_i.

2.3 Simplified computation of the transfer matrix

The computations can be simplified, and taken to larger strip widths, by utilizing the following general property of the eigenvalue structure of $\mathsf{T}(m)$:

1. All distinct eigenvalues of the block $T_{\ell,\ell}$ have the same amplitude, henceforth denoted $\alpha^{(\ell)}$, which is given by Eq. (2.25) below.

This property is an analytical result originating from the representation theory of quantum groups [25, 26]. Before reviewing the arguments for it we shall pause to discuss its practical utility.

Property 1 implies that the chromatic polynomial can be written as

$$P_{m\times n}(q) \;=\; \sum_{\ell=0}^{m} \alpha^{(\ell)} \sum_{i=1}^{L_\ell} \left(\lambda_\ell^{(i)}\right)^n \;, \tag{2.24}$$

where L_ℓ is the number of distinct eigenvalues in the block $T_{\ell,\ell}$ (see Table 3). Note that we have labeled the eigenvalues as $\lambda_\ell^{(i)}$, with ℓ being the corresponding number of bridges.

One important consequence of Eq. (2.24) is that in order to obtain all the eigenvalues and amplitudes we do no longer need to compute the full transfer matrix $\mathsf{T}(m)$. Rather, it is sufficient to diagonalize the blocks $T_{\ell,\ell}$ for $\ell = 0, 1, \ldots, m$ to get the eigenvalues $\lambda_\ell^{(j)}$ $(j = 1, \ldots, L_\ell)$ — assuming, of course, that we can determine the amplitudes $\alpha^{(\ell)}$ by some other method.

Property 1 and the exact expression of the amplitudes $\alpha^{(\ell)}$ follow from the presence of a quantum-group symmetry in the square-lattice Potts model [25, 26]. As a first step, the Potts model is reformulated as a six-vertex model in a standard way [28], the cyclic boundary conditions being imposed by the insertion of an appropriate twist operator [26]. It is then realized that the vertex model transfer matrix $\mathsf{T}_{\text{vertex}}$ commutes with the generators of the quantum algebra $\mathrm{U}_{\bar{q}}\,\mathrm{sl}(2)$ [25, 26], with deformation parameter $\bar{q}$ given by $\sqrt{q} = \bar{q} + 1/\bar{q}$. Decomposing the representation space into a direct sum over eigenspaces corresponding to each value of the vertex-model spin (which in turn is identified with ℓ) gives Property 1, along with the expression

$$\alpha^{(\ell)} \;=\; U_{2\ell}\left(\frac{\sqrt{q}}{2}\right) \;. \tag{2.25}$$

where $U_n(x)$ is the Chebyshev polynomial of the second kind, defined by [45],

$$U_n(x) \;=\; \frac{(x+i\sqrt{1-x^2})^{n+1} - (x-i\sqrt{1-x^2})^{n+1}}{2i\sqrt{1-x^2}} \;=\; \sum_{j=0}^{\lfloor n/2 \rfloor} (-1)^j \binom{n-j}{j} (2x)^{n-2j} \tag{2.26}$$

The form (2.25) has recently been rediscovered independently by Chang and Shrock [43], using arguments based on Temperley–Lieb algebra. Though the reasoning in [25, 26] and [43] may not constitute fully mathematically rigorous proofs, there is hardly any doubt that the results are correct. We have also verified Property 1 explicitly for strip widths $m \le 6$.

The first coefficients $\alpha^{(\ell)}$ are given by

$$\alpha^{(0)} = 1 \tag{2.27a}$$
$$\alpha^{(1)} = q - 1 \tag{2.27b}$$
$$\alpha^{(2)} = q^2 - 3q + 1 \tag{2.27c}$$
$$\alpha^{(3)} = q^3 - 5q^2 + 6q - 1 \tag{2.27d}$$
$$\alpha^{(4)} = (q-1)(q^3 - 6q^2 + 9q - 1) \tag{2.27e}$$

Another useful characterization of the amplitudes is the following [43]:

$$\alpha^{(\ell)} = \prod_{j=1}^{\ell} \left(q - B_{2\ell+1}^{(j)} \right) \tag{2.28}$$

where $B_n^{(j)}$ is the generalized Beraha number[8]

$$B_n^{(j)} = 4\cos^2\left(\frac{j\pi}{n}\right) = 2 + 2\cos\left(\frac{2\pi j}{n}\right) \tag{2.29}$$

and ℓ ranges between 0 and the strip width m. The standard Beraha numbers are $B_n \equiv B_n^{(1)}$.

In the case of the Potts model at general temperature, and generic values of $\bar{q}$, the representation theory for $\mathrm{U}_{\bar{q}}\,\mathrm{sl}(2)$ also fixes the dimension of the spin ℓ eigenspaces as $\binom{2m}{m-\ell} - \binom{2m}{m-\ell-1}$ [25, 26]. This formula should be compared with Table II in [46]. Note however that this is not equal to the number of distinct eigenvalues L_ℓ in the spin ℓ sector of (2.24). There are two reasons for this: 1) we are here considering the special case of the chromatic polynomial, for which many eigenvalues vanish due to the non-nearest-neighbor constraint (see Table 3), and 2) by symmetrizing with respect to reflections of the strip we have paired eigenstates whose eigenvalues would otherwise have been degenerate.

Let us stress that we have verified that Property 1 is in perfect agreement with all our exact transfer matrices up to strip width $m = 6$. Actually, this empirical evidence for $2 \le m \le 6$ verifies a slightly stronger property, which we state here as a conjecture:

2. Two distinct blocks $T_{\ell,\ell}$ and $T_{\ell',\ell'}$ (with $\ell \neq \ell'$), cf. (2.19), have no common eigenvalue. In other words, there does not exist ℓ, ℓ', i, i' such that $\lambda_\ell^{(i)} = \lambda_{\ell'}^{(i')}$ and $\ell \neq \ell'$.

Note that only Property 1 is necessary for making our simplified computation of the transfer matrix work. However, we have rather strong reasons for believing that Property 2 is actually true in general, since it essentially states that the combined $\mathrm{U}_{\bar{q}}\,\mathrm{sl}(2)$ and reflection (in the case of the square lattice) symmetries provides a *complete* identification of all the symmetries in the problem. We leave the question whether Property 2 can be proved by quantum-group techniques aside for a separate publication. Note that Property 2 with Eq. (2.24) would imply that $\sum_{\ell=0}^{m} L_\ell = \mathrm{SqRing}'(m)$, cf. Eqs. (2.15)–(2.16). And also note that Property 2 with Eq. (2.28) and the Beraha–Kahane–Weiss theorem [34] would imply that the only possible

[8]Note that $q = B_n^{(j)}$ with n, j integer corresponds to the quantum-group deformation parameter $\bar{q}$ being a rational-order root of unity, $\bar{q} = \mathrm{e}^{i\pi j/n}$.

real or complex isolated limiting points for cyclic strips of the triangular and square lattices are odd-n generalized Beraha numbers.[9] The fact that we observe exactly this structure of isolated limiting points also for $m = 7$ lends further credibility to Property 2.

From the point of view of computing the transfer matrix, further efficiency is achieved by making a further empirical observation (based on the strips of widths $2 \le m \le 6$):

3. Let T_{ℓ,ℓ,j_0} be any sub-block of $T_{\ell,\ell}$, cf. (2.20), whose dimension is the largest possible (there may be more than one such sub-block). Then the dimension of T_{ℓ,ℓ,j_0} is exactly L_ℓ, and all of its eigenvalues are distinct.

The dimensions of these sub-blocks are given by the L_ℓ in Table 2.

The characterization of the sub-blocks T_{ℓ,ℓ,j_0} with maximal dimension is interesting from a computational point of view. In particular, we have found that, for a given value of the number of bridges ℓ, the sub-blocks T_{ℓ,ℓ,j_0} split into two classes depending on whether the bottom-row connectivity $\mathcal{P}_{\text{bottom}}$ and the relative position of the ℓ bridges is symmetric or not under reflections. Let us denote those classes as $\mathcal{C}_{\text{sym}}$ and $\mathcal{C}_{\text{non-sym}}$, respectively. Then, we have empirically found for $2 \le m \le 8$ that: a) All blocks belonging to class $\mathcal{C}_{\text{sym}}$ have the same dimension L_{sym}; b) All blocks belonging to class $\mathcal{C}_{\text{non-sym}}$ have the same dimension $L_{\text{non-sym}}$; and c) $L_{\text{non-sym}} > L_{\text{sym}}$. Thus, any block belonging to the non-symmetric class $\mathcal{C}_{\text{non-sym}}$ is a maximal one with $L_{\text{non-sym}} = L_\ell$ (see Table 3). The only exception to this rule occurs when the non-symmetric class is empty $\mathcal{C}_{\text{non-sym}} = \varnothing$. In this particular case, any block belonging to $\mathcal{C}_{\text{sym}}$ is a maximal one with $L_\ell = L_{\text{sym}}$. For instance, for a strip of width $m \ge 3$, we can always choose as maximal blocks with $k = 1, \ldots, m$ bridges those blocks characterized by $\mathcal{P}_{\text{bottom}} = 1$ (i.e., no connections among the sites of the bottom rim) and bridges located at sites $1', \ldots, k'$. Finally, we can choose as maximal block with no bridges ($\ell = 0$) the block with $\mathcal{P}_{\text{bottom}} = \delta_{1',3'}$.

Note that Property 3 is not very surprising at all when one recalls that j_0 labels the bottom-row connectivities. Since the transfer matrix acts on top-row connectivities only, one would not expect its spectrum to depend on j_0 (apart from the reflection parity effect observed above). To save space we refrain from turning this idea into a formal proof.

Supposing Property 3 to be true in general, it suffices to diagonalize one maximal sub-block for each $\ell = 0, 1, \ldots, m$ (e.g., those described above). This method has allowed us to extend our results up to $m = 8$.

An important question is whether this procedure is able to give *all* the $\text{SqRing}'(m)$ distinct eigenvalues of the transfer matrix $\mathsf{T}(m)$. For the strips of widths $2 \le m \le 6$, we have explicitly verified that this is the case, as we can handle the full transfer matrix (See Section 2.2). For widths $m = 7, 8$, the situation is apparently less clear. In Table 3 we have displayed the dimension $L_\ell(m)$ of the maximal block $\mathsf{T}_{\ell,\ell,j_0}(m)$ for a strip of width m with ℓ bridges. These numbers fully agree with the *exact* number of distinct eigenvalues $n_P(m, \ell)$ in the corresponding ℓ-bridge subspace found by Chang and Shrock [43, Table 1]. Thus, we can guarantee that for $m = 7, 8$ we have not missed any transfer-matrix eigenvalue, and that our results are indeed exact. Furthermore, the total number of distinct eigenvalues we have found is equal to the predicted number $\text{SqFree}'(m)$ [43].

[9] The position of the isolated limiting points depends on the boundary conditions of the strips. For square-lattice strips with free and cylindrical boundary conditions [22, 23] we have found that (at least up to widths $m = 12$) all Beraha numbers up to $B_6 = 3$ (and only those) can be isolated limiting points. Furthermore, we have found complex-conjugate pairs of complex isolated limiting points.

Remark. We stress that the results for widths $2 \le m \le 6$ have been obtained completely *ab initio*, using the practical procedure described in Section 2.2. Thus, for these strips, we have not used any unproven property. For the strips of widths $m = 7, 8$, we have used the simplified method described above, which makes use of Properties 1 and 3. Property 2 is actually not needed and used in our practical procedure.

3 Square-lattice chromatic polynomials with cyclic boundary conditions

In this section we will analyze the results for the square-lattice strips of widths $2 \le L \le 8$. Even though the two smaller strips ($L = 2, 3$) are well known in the literature, we will describe them in detail using our approach. The other cases published in the literature $L = 4, 5$ will be briefly reviewed for completeness. Finally, our new results will be described in detail. A summary of the main characteristics of the limiting curves for these strips is displayed in Table 4. Finally, in Table 5 we list the real chromatic zeros for square-lattice strips of size $L_{\rm F} \times (kL)_{\rm P}$ with $1 \le k \le 10$.

For the larger L, we have not attempted to write the complete analytic expressions for the eigenvalues and amplitudes in this paper, as they are rather lengthy. The interested reader can find them in the MATHEMATICA file `transfer4_sq.m` available as part of the electronic version of this paper in the `cond-mat` archive. The analytic expressions for the sub-blocks T_{ℓ,ℓ,j_0} can be obtained by request from the authors.

3.1 $L = 2$

This case was first solved by Biggs, Damerell and Sands back in 1972 [35]. Their solution is

$$P_{2\times n}(q) \;=\; (q^2-3q+3)^n + (q-1)\left[(3-q)^n + (1-q)^n\right] + q^2 - 3q + 1 \tag{3.1}$$

Let us review our derivation of this result. The transfer matrix $\mathsf{T}(2)$ has dimension four. In the basis $\{\delta_{1,1'}\delta_{2,2'}, \delta_{1,1'} + \delta_{2,2'}, \delta_{1,2'} + \delta_{2,1'}, 1\}$, it takes the form

$$\mathsf{T}(2) \;=\; \left(\begin{array}{c|cc|c} 1 & 0 & 0 & 0 \\ \hline -1 & 2-q & 1 & 0 \\ 0 & 1 & 2-q & 0 \\ \hline 1 & 2(q-2) & 2(q-2) & q^2-3q+3 \end{array}\right) \tag{3.2}$$

where we by vertical and horizontal lines show the block structure of this matrix (see below). We have ordered the basis elements according to a decreasing number of bridges so that the matrix (3.2) shows clearly its lower-triangular block form. The right $\boldsymbol{w}_{\rm id}$ and left $\boldsymbol{u}$ vectors are given by

$$\boldsymbol{u}^T \;=\; (A, 2A, 0, A)\,, \qquad \text{with } A = q(q-1) \tag{3.3a}$$

$$\boldsymbol{w}_{\rm id}^T \;=\; (1, 0, 0, 0) \tag{3.3b}$$

The transfer matrix (3.2) can be decomposed into three blocks: all of them are characterized by the same bottom-row connectivity ($\mathcal{P}_{\rm bottom} = 1$, i.e., there is no connection between

the sites $1'$ and $2'$). In this case, the difference between blocks is solely due to the number of bridges ℓ connecting the top and bottom rows.

The first block is one-dimensional and corresponds to the connectivity state $\delta_{1,1'}\delta_{2,2'}$ (thus, $\ell = 2$). The eigenvalue is

$$\lambda_{\ell=2} \;=\; 1 \tag{3.4}$$

The third block is also one-dimensional and it corresponds to the singleton state 1. Thus, it is characterized by zero bridges ($\ell = 0$). The eigenvalue is

$$\lambda_{\ell=0} \;=\; q^2 - 3q + 3 \tag{3.5}$$

Finally, the second block corresponds to the two remaining states, and it is characterized by a single bridge ($\ell = 1$). The eigenvalues of this block are

$$\lambda_{\ell=1}^{(1)} \;=\; 3 - q \tag{3.6a}$$
$$\lambda_{\ell=1}^{(2)} \;=\; 1 - q \tag{3.6b}$$

The amplitudes associated to those eigenvalues are given by [c.f. (2.27)]

$$\alpha_{\ell=2} \;=\; \alpha^{(2)} \tag{3.7a}$$
$$\alpha_{\ell=1}^{(j)} \;=\; \alpha^{(1)}\,, \quad j = 1,2 \tag{3.7b}$$
$$\alpha_{\ell=0} \;=\; \alpha^{(0)} = 1 \tag{3.7c}$$

where the $\alpha^{(j)}$ are given by (2.25), in full agreement with the exact result (3.1). As discussed in Section 2.3, the amplitude $\alpha^{(\ell)}$ is associated to every eigenvalue $\lambda_\ell^{(i)}$ coming from the block $T_{\ell,\ell}$.

We have depicted the chromatic zeros for the square-lattice strips of width $L = 2_{\rm F}$ and lengths $n = 10_{\rm P}, 20_{\rm P}$ in Figure 3(a). We have also depicted the limiting curve $\mathcal{B}$ for this strip.[10] This curve was computed using the resultant method (see, e.g., [22]). It divides the complex q-plane into four regions, and crosses the real q-axis at $q = 0, 2$. At this latter point it has a quadruple point. There are also two T points at $q = 2 \pm \sqrt{2}$.

The isolated limiting points are very easy to locate as the amplitudes have a simple analytic form (2.28): there is a single isolated limiting point at $q = 1$.

3.2 $L = 3$

The solution for this strip was first found by Shrock and Tsai in 2000 [36]:

$$\begin{aligned} P_{3\times n}(q) \;=\; & (q^3 - 5q^2 + 6q - 1)(-1)^n + (q^2 - 3q + 1)\left[(q-1)^n + (q-2)^n + (q-4)^n\right] \\ & +(q-1)\left[\left(-(q-2)^2\right)^n + \sum_{i=6}^{8} \lambda_i^n\right] + \sum_{i=9}^{10} \lambda_i^n \end{aligned} \tag{3.8}$$

where the λ_i for $i = 9, 10$ are the solutions of the equation

$$x^2 - (q-2)(q^2 - 3q + 5)x + (q-1)(q^3 - 6q^2 + 13q - 11) \;=\; 0 \tag{3.9}$$

[10] The limiting curve for a square-lattice strip of width $L = 2$ and cyclic boundary conditions was first computed by Biggs, Damerell and Sands [35]. We include it here to compare it to the new results presented in this paper.

and those for $i = 6, 7, 8$ are the solutions of the third-order equation

$$\begin{aligned} x^3 \;+\; (2q^2 - 9q + 12)x^2 + (q^4 - 10q^3 + 36q^2 - 56q + 31)x \;=& \\ (q-1)(q^4 - 9q^3 + 29q^2 - 40q + 22) & \end{aligned} \tag{3.10}$$

We have re-derived the above result using our method. The transfer matrix is 20-dimensional, and can be split into eight blocks. The diagonalization of these blocks lead to the eigenvalues given in (3.8). We have also confirmed that the amplitudes are precisely those given by (3.8).

There is a single block for $\ell = 3$ bridges. Its eigenvalue is $\lambda_{\ell=3} = -1$ and its amplitude is $\alpha^{(3)}$. We also find two blocks with $\ell = 2$. The corresponding eigenvalues are $\lambda^{(j)}_{\ell=2} = q-4, q-2, q-1$, and their amplitude is $\alpha^{(2)}$. There are three blocks with a single bridge ($\ell = 1$). The eigenvalues are $\lambda^{(1)}_{\ell=1} = -(q-2)^2$ and $\lambda^{(j=2,3,4)}_{\ell=1}$ are the solutions of the third-order equation (3.10). The amplitude is $\alpha^{(1)}$ for these four eigenvalues. Finally, there are two blocks with no bridges $\ell = 0$; their eigenvalues are the solutions of the second-order equation (3.9), and $\alpha^{(0)}$ is their amplitude.

The chromatic zeros for the square-lattice strips of width $L = 3_{\rm F}$ and lengths $n = 15_{\rm P}, 30_{\rm P}$ are displayed in Figure 3(b). The limiting curve $\mathcal{B}$ (computed with the resultant method) is also depicted in that figure. This curve was first obtained by Shrock and Tsai [36].

The limiting curve crosses the real q-axis at $q = 0, 2$ and $q \approx 2.3365442725$. We find ten T points at $q \approx 1.7713445981 \pm 1.7900810556\,i$, $q \approx 2.0457165736 \pm 1.6008334033\,i$, $q \approx 2.2701797354 \pm 0.9704300675\,i$, $q \approx 2.0401211769 \pm 1.6256019349\,i$, and $q \approx 2.3527863293 \pm 0.3787883673\,i$. We also find a single isolated limiting point at $q = 1$.

3.3 $L = 4$ and $L = 5$

The solution for $L = 4$ was obtained by Chang and Shrock [37]. We have re-derived their result by using our approach. The transfer matrix has dimension 94, and it can be split into 16 blocks. After obtaining the eigenvalues of all such blocks, we arrive at the 26 distinct eigenvalues and amplitudes found by Chang and Shrock [37]. These eigenvalues and amplitudes have the structure described in Section 2.3.

In Figure 3(c) we show the chromatic zeros for strips of sizes $4_{\rm F} \times 20_{\rm P}$ and $4_{\rm F} \times 40_{\rm P}$, as well as the limiting curve $\mathcal{B}$.[11] The computation of this curve was done by means of the direct-search method (see e.g. [22]). Thus, the number of relevant features reported below should be regarded as lower bounds. The limiting curve $\mathcal{B}$ crosses the real q-axis at three points: $q = 0, 2$, and $q \approx 2.4928455591$. We have found six T points at $q \approx 2.2192166698 \pm 1.5778851486\,i$, $q \approx 2.3408741083 \pm 1.3290891386\,i$, and $q \approx 2.5035997660 \pm 0.4577795448\,i$. As in the previous strips, there is a single isolated limiting point at $q = 1$.

The solution for $L = 5$ was found by Chang and Shrock [38]. The full transfer matrix has dimension 614, and it can be split into 44 blocks. From them we have obtained the 70 distinct eigenvalues and their associated amplitudes. Again we find the eigenvalue and amplitude structure discussed in Section 2.3.

[11] Although the limiting curve for this lattice was not included in the original reference by Chang and Shrock [37], it appeared in the subsequent paper [38] by the same authors.

In Figure 3(d) we depict the chromatic zeros for the strips of length $n = 25_{\rm P}, 50_{\rm F}$. We also plot the limiting curve $\mathcal{B}$, which was computed using the direct-search method.[12] This curve $\mathcal{B}$ crosses the real q-axis at $q = 0, 2$ and $q \approx 2.5823854661$. We have found six T points at $q \approx 2.3986403427 \pm 1.4510688289\,i$, $q \approx 2.5948107219 \pm 0.4767225937\,i$, and $q \approx 2.2911897201 \pm 1.6493441205\,i$. Finally, there is a single isolated limiting point at $q = 1$.

3.4 $L = 6$

The full transfer matrix $\mathsf{T}(6)$ has dimension 4028, and can be split into 105 blocks. After performing the diagonalization of these blocks, we have found 192 distinct eigenvalues (in agreement with Eq. (2.15)). The solution can be written in the form

$$P_{6\times n}(q) \;=\; \sum_{i=1}^{192} \alpha_i(q)\lambda_i(q)^n \tag{3.11}$$

We find several simple eigenvalues: e.g. $\lambda = 1$, $\lambda = 4-q, 3-q, 2-q, 1-q$. The other eigenvalues come from solving polynomic equations up to order 30. We find the same structure of the eigenvalues and amplitudes in terms of the number of bridges ℓ as for the other strips.

In Figure 4(a) we show the chromatic zeros for the lengths $30_{\rm P}$ and $60_{\rm P}$, and the limiting curve $\mathcal{B}$. This curve has been computed using the direct-search method. Thus, the number of T points and the other features discussed below should be taken as lower bounds of the true values.

The limiting curve $\mathcal{B}$ crosses the real q-axis at $q = 0, 2$ and $q = q_0 \approx 2.6460783059$. We have found 10 T points at $q \approx 2.3494422185 \pm 1.6759458630\,i$, $q \approx 2.3716213974 \pm 1.6415616784\,i$, $q \approx 2.4271173045 \pm 1.5496869588\,i$, $q \approx 2.4988088784 \pm 1.4046791200\,i$, and $q \approx 2.6565980229 \pm 0.4807158507\,i$. There are two small triangular-like regions delimited by the six T points around $q \approx 2.37 \pm 1.64\,i$. In total, there are six enclosed regions in the complex q-plane; only two of them have non-void intersection with the real q-axis.

There are two isolated limiting points at $q = 1$ and $q = B_5$, as the value of q_0 is larger than B_5. This is the smallest width for which we find two isolated limiting points among the square-lattice strips considered in this paper.

We remark that the limiting curve crosses the real q-axis at $q_0 \approx 2.6460783059 > B_5$. Thus, in principle there could be real zeros larger than $q = B_5$ (See Table 5).[13] However, we computed the zeros of $P_{6\times n}(q)$ up to $n = 60$ and did not find any real zeros larger than B_5. This point is relevant in relation to a conjecture by Woodall [47], stating that no bipartite planar graph can have a real chromatic zero greater than $q = 2$. This conjecture was disproved in ref. [22], and modified in the following way: for any bipartite planar graph G, $P_G(q) > 0$ for all real $q \geq B_5$ [22, Conjecture 7.5].

[12] This limiting curve was first obtained by Chang and Shrock [38].

[13] In refs. [22, 23] it was found that for square-lattice strips with cylindrical boundary conditions and even width $L = 8, 10, 12$, the limiting curve $\mathcal{B}$ does not cross the real q-axis. Indeed, for $L = 4, 6$, $\mathcal{B}$ crosses the real q-axis at $q_0 < B_5$. No chromatic real root greater than B_5 was found.

3.5 $L = 7$

The full transfer matrix $\mathsf{T}(7)$ has dimension 28940, and can be split into 294 blocks (see Table 2). The computation of such an enormous symbolic matrix is beyond our current computer facilities. However, using the simplified method described in Section 2.3, we have been able to obtain the diagonal blocks T_{ℓ,ℓ,j_0} (i.e., for each number of bridges $\ell = 0, \ldots, 7$, we choose among all possible sub-blocks of $T_{\ell,\ell}$ one with the largest possible dimension given by L_ℓ in Table 3).

The blocks T_{ℓ,ℓ,j_0} are themselves large: their dimensions range from 1 to 145. This fact severely limits the applicability of the method: we have been unable to compute the characteristic polynomial of any block of dimension larger than 100. Thus, with our current computer facilities, we cannot obtain closed formulas for the eigenvalues (as in the preceding cases). This implies that we cannot compute the chromatic polynomial for this strip family. However, we are able to compute the limiting curve (which depends only on the eigenvalues provided none of the amplitudes α_k vanishes identically) by the direct-search method combined with *numerical* determination of the eigenvalues at any given q.

In Figure 4(b) we show the zeros for a square-lattice strip of size $7_{\mathrm{F}} \times 7_{\mathrm{P}}$ (obtained using Eq. (2.18) and previous results for cylindrical boundary conditions [22]). We also show the limiting curve $\mathcal{B}$; it has been computed using the direct-search method. The computation of this curve is more involved than for the previous cases, as we do not have the chromatic zeros to guide our search. Thus, the number of T points and the other features discussed below should be taken as lower bounds of the true values.

The limiting curve $\mathcal{B}$ crosses the real q-axis at $q = 0, 2$ and $q = q_0 \approx 2.6927280047$. We have found 14 T points at $q \approx 2.4008837606 \pm 1.6805209516\,i$, $q \approx 2.5993953677 \pm 1.2843636999\,i$, $q \approx 2.7015691600 \pm 0.4815451956\,i$, $q \approx 2.7022195651 \pm 0.9476253694\,i$, $q \approx 2.7126320142 \pm 0.8591968848\,i$, $q \approx 2.7152854276 \pm 0.7936937430\,i$, and $q \approx 2.7248651978 \pm 0.8452059951\,i$.

There are two tiny complex-conjugate features of the limiting curve that are not visible in Figure 4(b). Around $q \approx 2.71 \pm 0.85$, we find two closed regions delimited by the T points $q \approx 2.7022195651 \pm 0.9476253694\,i$ and $q \approx 2.7152854276 \pm 0.7936937430\,i$. These regions are split in two by small lines connecting the T points $q \approx 2.7248651978 \pm 0.8452059951\,i$ and $q \approx 2.7126320142 \pm 0.8591968848\,i$. Thus, we find four small closed regions delimited by the latter four T points listed above.

There are two isolated limiting points at $q = 1$ and $q = B_5$, as the value of q_0 is larger than B_5.

3.6 $L = 8$

The full transfer matrix $\mathsf{T}(8)$ has dimension 212370, and can be split into 777 blocks (see Table 2). We have been unable to compute this huge symbolic matrix. By using the method described in Section 2.3, we have been able to obtain the nine diagonal blocks T_{ℓ,ℓ,j_0}. Several blocks T_{ℓ,ℓ,j_0} are still very large: their dimensions range from 1 to 385. Again, we cannot compute the symbolic characteristic polynomial of the largest sub-blocks, and hence, the chromatic polynomial. But the numerical computation of the eigenvalues is possible, but very time consuming. This is the reason we have not tried to determine the whole limiting curve $\mathcal{B}$. The only exception is the determination of the value of q_0 for this strip family:

$q_0 \approx 2.7287513178$. Finally, we expect two isolated limiting points at $q = 1$ and $q = B_5$, as the value of q_0 is larger than B_5.

4 Transfer matrix for triangular-lattice strips with cyclic boundary conditions

The results are very similar to those obtained for the square lattice in Section 2. The transfer matrix is written as

$$\mathsf{T}(m) \;=\; \mathsf{V}(m) \cdot \mathsf{H}(m) \tag{4.1}$$

with the same formula for $\mathsf{H}(m)$ (2.4a), but a different one for the "vertical-bond" matrix $\mathsf{V}(m)$:

$$\mathsf{V}(m) \;=\; \mathsf{P}_m \cdot \mathsf{Q}_{m,m-1} \cdot \mathsf{P}_{m-1} \cdot \ldots \cdot \mathsf{Q}_{2,1} \cdot \mathsf{P}_1 \tag{4.2}$$

In Figure 5 we show the construction of a 4×2 triangular-lattice strip.

The chromatic polynomial is given by the same formulas as for the square lattice (2.5)/(2.12). Again we choose to work with the connectivity basis $\widetilde{\boldsymbol{w}}_{\mathcal{P}} = \mathsf{H}(m) \cdot \mathsf{H}'(m) \cdot \boldsymbol{v}_{\mathcal{P}}$, as $\widetilde{\boldsymbol{w}}_{\mathcal{P}} = 0$ for all partitions $\mathcal{P}$ that contain two nearest-neighbor sites (on either the top or the bottom rows) in the same block. This basis has dimension TriRing(m) for a strip of width m (see Table 1).

There is no reflection symmetry for a triangular-lattice strip, so the dimension of the transfer matrix is TriRing(m). However, the number of distinct eigenvalues should be the same as for the square lattice, viz. SqRing$'(m)$ in Table 1, as the underlying $\mathrm{U}_{\bar{q}}\,\mathrm{sl}(2)$ quantum-group symmetry is the same [26]. That this is indeed the case has been checked explicitly by Chang and Shrock [43].

Also in the triangular-lattice case, the quantum-group symmetry ensures that the chromatic polynomial for a strip of size $m \times n$ can be written as in (2.24). Again, this means that only odd-n generalized Beraha numbers can be isolated limiting points.[14]

The block structure of $\mathsf{T}(m)$ is similar to that of the square-lattice case (2.19)/(2.20). The only difference is that the triangular lattice is not invariant under reflections with respect to the center of the strip. Thus, for a given number of bridges ℓ, we expect that the number of blocks N_ℓ is larger than for the square case (see Table 3). Indeed, for all $m \le 8$, and for any ℓ, we empirically find that N_ℓ coincides with the number of distinct eigenvalues L_ℓ coming from $T_{\ell,\ell}$, and that all the N_ℓ blocks have the same dimension L_ℓ (see Table 3). Thus, we conclude that for $m \le 8$

$$\sum_{\ell=0}^{m} L_\ell^2 \;=\; \mathrm{TriRing}(m) \tag{4.3}$$

[14] For triangular-lattice strips with free and cylindrical boundary conditions, we have found that *all* Beraha numbers up to B_{10} are isolated limiting points [24] (at least up to widths $m = 12$). There are two different conjectures about how many Beraha numbers can be isolated limiting points for this lattice. Baxter's results [21]) imply that all Beraha numbers up to (and including) B_{14} should be isolated limiting points for large enough widths m. The reanalysis of Baxter's solution [24] led us to a new conjecture: only the Beraha numbers up to B_{11} (and possibly B_{12}) can be isolated limiting points. In addition to these issues, we have found that for strips with free and cylindrical there are no complex isolated limiting points up to widths $m = 12$. However, for "zig-zag" boundary conditions, we found complex isolated limiting points, and, more importantly, real isolated limiting points that are *not* Beraha numbers (e.g., $q = 5/2$).

and we conjecture that this equation holds for arbitrary values of m.

Once again, the form (2.24) allows us to make computations for widths $m > 6$. Since all the sub-blocks $T_{\ell,\ell,j}$ are expected to have the same dimension, we can choose any of them to perform the computations using the simplified method described in Section 2.3.

Remarks: 1. As for the square-lattice case, we have checked our results with the help of the available results for triangular-lattice strips with cylindrical boundary conditions [c.f., Eq. (2.18)].

2. As for the square-lattice case, the transfer matrices for the strips of widths $m \leq 6$ have been obtained without using any unproven property. For $m = 7, 8$ we have used Properties 1 and 3 of Section 2.3 to obtain *all* the eigenvalues. For each block $T_{\ell,\ell}$, we have obtained $L_\ell(m)$ distinct eigenvalues (See Table 3), where L_ℓ coincides with the predicted number of distinct eigenvalues for the sector with ℓ bridges [41, Table1].

5 Triangular-lattice chromatic polynomials with cyclic boundary conditions

In this section we will analyze the results for the triangular-lattice strips of widths $2 \leq L \leq 8$. As in Section 3, we will describe our methods on the smaller widths $L = 2, 3$, briefly review (for completeness) the already-known cases ($L = 4$), and describe in detail the new results presented in this section ($L \geq 5$). In Table 6 we list the real chromatic zeros for triangular-lattice strips of size $L_{\rm F} \times (kL)_{\rm P}$ with $1 \leq k \leq 10$. A summary of the main characteristics of the limiting curves for these strips is displayed in Table 7.

The interested reader can find the analytic expressions for the eigenvalues and amplitudes for all lattices reported in this section in the MATHEMATICA file `transfer4_tri.m` available as part of the electronic version of this paper in the `cond-mat` archive. The analytic expressions for the sub-blocks T_{ℓ,ℓ,j_0} can be obtained from the authors.

5.1 $L = 2$

This case was first solved by Tsai and Shrock [36]. The solution is

$$P_{2\times n}(q) \;=\; (q^2-3q+1) + (q-2)^{2m} + (q-1)\left[\lambda_3^n + \lambda_4^n\right] \tag{5.1}$$

where $\lambda_{3,4}$ are the solutions of the equation

$$(q-2)^2 + (2q-5)x + x^2 \;=\; 0 \tag{5.2}$$

Let us review our derivation of this result. The transfer matrix has dimension six. In the basis $\{\delta_{1,1'}\delta_{2,2'}, \delta_{1,2'}, \delta_{2,2'}, \delta_{1,1'}, \delta_{2,1'}, 1\}$, it takes the form

$$\mathsf{T}(2) \;=\; \left(\begin{array}{c|cc|cc|c} 1 & 0 & 0 & 0 & 0 & 0 \\ \hline 0 & 2-q & 1 & 0 & 0 & 0 \\ -1 & 2-q & 3-q & 0 & 0 & 0 \\ \hline -1 & 0 & 0 & 2-q & 1 & 0 \\ -1 & 0 & 0 & 2-q & 3-q & 0 \\ \hline 1 & q-2 & q-3 & q-2 & q-3 & (q-2)^2 \end{array}\right) \tag{5.3}$$

where the vertical and horizontal lines show the block structure of this matrix (see below). The right $\boldsymbol{w}_{\rm id}$ and left $\boldsymbol{u}$ vectors are given by

$$\boldsymbol{u}^T = (A, 0, A, A, 0, A)\,, \qquad \text{with } A = q(q-1) \tag{5.4a}$$

$$\boldsymbol{w}_{\rm id}^T = (1, 0, 0, 0, 0, 0) \tag{5.4b}$$

Again, we have arranged the basis elements in decreasing order of number of bridges ℓ, so the lower-triangular block form of $\mathsf{T}(2)$ becomes apparent.

The full transfer matrix can be decomposed into four blocks: as in the square-lattice case with $L = 2$, all of them are characterized by the same bottom-row connectivity $\mathcal{P}_{\rm bottom} = 1$, and differ only by the number of bridges ℓ. The first block is one-dimensional and it corresponds to the connectivity state with $\ell = 2$ bridges. Its eigenvalue is

$$\lambda_{\ell=2} = 1 \tag{5.5}$$

The fourth block is also one-dimensional and corresponds to $\ell = 0$ bridges. Its eigenvalue is

$$\lambda_{\ell=0} = (q-2)^2 \tag{5.6}$$

The second and third blocks are identical two-dimensional blocks corresponding to a single bridge $\ell = 1$: for the former block it emerges at site $2'$, and for the latter one it emerges at site $1'$. Their eigenvalues $\lambda_{\ell=1}^{(j)}$ $(j = 1, 2)$ are given by the solutions of the second-order equation (5.2). Please note that the block $T_{1,1}$ is block diagonal as discussed in Section 2.2.

We have computed the amplitudes in the same way as for the square lattice. The results are given by [c.f. (2.27)]

$$\alpha_{\ell=2} = \alpha^{(2)} \tag{5.7a}$$

$$\alpha_{\ell=1}^{(j)} = \alpha^{(1)}\,, \qquad j = 1, 2 \tag{5.7b}$$

$$\alpha_{\ell=0} = \alpha^{(0)} = 1 \tag{5.7c}$$

These formulas agree with the already known exact results (5.1)/(5.2). Again, the amplitude associated to each eigenvalue $\lambda_\ell^{(j)}$ coming from block $T_{\ell,\ell}$ is $\alpha^{(\ell)}$.

We have depicted the chromatic zeros for the triangular-lattice strips of width $L = 2_{\rm F}$ and lengths $n = 10_{\rm P}, 20_{\rm P}$ in Figure 6(a). The limiting curve $\mathcal{B}$ for this strip is also shown. This curve has been obtained using the resultant method.[15] It crosses the real q-axis at $q = 0, 2, 3$. At this latter point it has a quadruple point. The limiting curve divides the complex q-plane into three closed regions. Finally, there are two isolated limiting points at $q = 1$ and $q = B_5$.

5.2 $L = 3$

This case was first solved by Chang and Shrock [39], who also computed the limiting curve. We have re-derived their result using our method. The full transfer matrix has dimension 30. It can be split into ten different blocks. These blocks provide the ten distinct

[15] This limiting curve was first obtained by Shrock and Tsai [36].

eigenvalues of the transfer matrix. Following a similar procedure as for the square-lattice strips we obtained the corresponding amplitudes.

There is a single block with $\ell = 3$ bridges: this is one-dimensional and it corresponds to the eigenvalue

$$\lambda_{\ell=3} \;=\; -1 \tag{5.8}$$

and its amplitude is $\alpha^{(3)}$. The block $T_{2,2}$ contains three identical sub-blocks, each of them leading to three distinct eigenvalues $\lambda_{\ell=2}^{(j=1,2,3)}$. The simplest one is

$$\lambda_{\ell=2}^{(1)} \;=\; q - 2 \;, \tag{5.9}$$

while the other two are the solutions of the second-order equation

$$x^2 - x(2q-7) + q^2 - 5q + 6 \;=\; 0 \;. \tag{5.10}$$

The amplitude associated to these eigenvalues is $\alpha^{(2)}$. We have also found four (identical) sub-blocks with a single bridge ($\ell = 1$). Each of them has four eigenvalues $\lambda_{\ell=3}^{(j)}$. The simplest one is

$$\lambda_{\ell=1}^{(1)} \;=\; -q^2 + 5q - 6 \tag{5.11}$$

and the other three are the solutions of the third-order equation

$$\begin{aligned} 0 \;=\; & x^3 + (2q^2 - 12q + 19)x^2 + (q^4 - 11q^3 + 46q^2 - 85q + 58)x \\ & -q^5 + 11q^4 - 48q^3 + 104q^2 - 112q + 48 \end{aligned} \tag{5.12}$$

The amplitude $\alpha^{(1)}$ corresponds to all of them. Finally, there are two (identical) sub-blocks characterized by no bridges ($\ell = 0$). Their eigenvalues are the solutions of the second-order equation

$$x^2 - x(q^3 - 7q^2 + 18q - 17) + q^4 - 9q^3 + 30q^2 - 44q + 24 \;=\; 0 \tag{5.13}$$

and their amplitudes are $\alpha^{(0)} = 1$.

In Figure 6(b) we show the chromatic zeros for the strips of sizes $3_{\rm F} \times 15_{\rm P}$ and $3_{\rm F} \times 15_{\rm P}$, and the limiting curve $\mathcal{B}$. This latter curve was obtained using the resultant method.[16] It crosses the real q-axis at $q = 0, 2, 3$. At this latter point the curve has a quadruple point. There are eight T points at $q \approx 2.2532978656 \pm 1.6576481039\,i$, $q \approx 3.1233767820 \pm 1.1226454338\,i$, $q \approx 3.1427903492 \pm 0.3662742838\,i$, and $q \approx 3.0244195343 \pm 0.1322645045\,i$. Finally, we find two isolated limiting points at $q = 1$ and $q = B_5$.

5.3 $L = 4$

This case was first solved by Chang and Shrock [39], who also computed the limiting curve. We have re-derived their result by using our general procedure. The full transfer matrix has dimension 178, and it can be split into 26 blocks.

In Figure 6(c) we show the chromatic zeros for the strips of sizes $4_{\rm F} \times 20_{\rm P}$ and $4_{\rm F} \times 40_{\rm P}$, and the limiting curve $\mathcal{B}$.[17] This latter curve was obtained using the direct-search method.

[16] The limiting curve for this strip was first computed by Chang and Shrock [39].

[17] The limiting curve for this strip was first computed by Chang and Shrock [39].

Thus, the number of endpoints and other features reported below should be interpreted as lower bounds of the true values.

The limiting curve $\mathcal{B}$ crosses the real q-axis at $q = 0, 2, 3$ and $q \approx 3.2281262261$. We have found eight T points at $q \approx 3.3762587794 \pm 0.9748801876\,i$, $q \approx 3.3525265561 \pm 0.5771942145\,i$, $q \approx 3.3542356970 \pm 0.5945094569\,i$, and $q \approx 1.4763063347 \pm 2.0348131808\,i$. There are two isolated limiting points at $q = 1, B_5$.

5.4 $L = 5$

After we completed the computation of this case we learned that it had been independently solved by Chang and Shrock [41]. Our result based on our transfer-matrix method fully agrees with theirs.

The full transfer matrix is 1158 dimensional, and can be split into 70 blocks. After the diagonalization of such blocks we find 70 different eigenvalues. Again, we find the eigenvalue/amplitude structure discussed in Section 2.3.

In Figure 7(a) we show the chromatic zeros for the strips of sizes $5_{\rm F} \times 25_{\rm P}$ and $5_{\rm F} \times 50_{\rm P}$, and the limiting curve $\mathcal{B}$. This latter curve was computed via the direct-search method.[18] The curve $\mathcal{B}$ has a more involved shape than for the other triangular-lattice strips with smaller width. It crosses the real q-axis at $q = 0, 2, 3$ and $q \approx 3.3324469422$. We have found 16 T points at $q \approx 1.0114299869 \pm 2.1132511328\,i$, $q \approx 1.1643009748 \pm 2.2002545351\,i$, $q \approx 2.5640974594 \pm 2.0365055771\,i$, $q \approx 2.5843109937 \pm 1.9725597103\,i$, $q \approx 2.6549519688 \pm 1.9693915215\,i$, $q \approx 3.4850579943 \pm 0.9796767236\,i$, $q \approx 3.5231420699 \pm 0.7322113419\,i$, and $q \approx 3.5309588080 \pm 0.8827974592\,i$. The unusual features are a) two tiny bulb-like regions protruding from the T points at $q \approx 1.0114299869 \pm 2.1132511328\,i$; and b) two small triangular-shaped regions delimited by the six T points around $q \approx 2.60 \pm 2.00\,i$.

Finally, there are three isolated limiting points at $q = 1, B_5$ and B_7. This is the triangular-lattice strip with smallest width for which we find an isolated limiting point at $q = B_7$.

5.5 $L = 6$

The full transfer matrix is 7986 dimensional, and can be split into 192 blocks. The diagonalization of these blocks leads to the 192 different eigenvalues, in agreement with the formula (2.15). The simplest eigenvalue is $\lambda = 1$ which comes from the block $T_{6,6}$; thus, its amplitude is $\alpha^{(6)}$. The other eigenvalues are given by the solution of polynomic equations up to order 55. We find the block structure of eigenvalues and amplitudes described in Section 2.3.

In Figure 7(b) we show the chromatic zeros for the strips of sizes $6_{\rm F} \times 30_{\rm P}$ and $6_{\rm F} \times 60_{\rm P}$, and the limiting curve $\mathcal{B}$. This latter curve was computed via the direct-search method. This curve crosses the real q-axis at $q = 0, 2, 3$ and $q \approx 3.4062849655$. We have found 10 T points at $q \approx 0.8028018425 \pm 2.2224309039\,i$, $q \approx 2.2195798331 \pm 2.3066154729\,i$, $q \approx 3.6219823536 \pm 0.8757610205\,i$, $q \approx 3.6246351106 \pm 0.8660035657\,i$, and $q \approx 3.6870064797 \pm 0.8100610005\,i$. There are two bulb-like regions emerging from the last T points ($q \approx 3.6870064797 \pm$

[18] The computation of this limiting curve is new, as it was not published in the (first) preprint version of Ref. [41].

$0.8100610005\,i$). We have also found two endpoints at[19] $q \approx 0.5716823545 \pm 1.9896139773\,i$. These points correspond to two complex-conjugate small branches protruding from the T points at $q \approx 0.8028018425 \pm 2.2224309039\,i$. This is first triangular-lattice strip for which we find endpoints. Finally, there are three isolated limiting points at $q = 1, B_5$ and B_7.

5.6 $L = 7$

The full transfer matrix $\mathsf{T}(7)$ has dimension 57346, and can be split into 534 blocks (see Table 3). By making use of the simplified method described in Section 2.3, we have obtained the relevant sub-blocks T_{ℓ,ℓ,j_0} from which all distinct eigenvalues can be computed.

Unfortunately, the sub-blocks T_{ℓ,ℓ,j_0} have rather large dimensions, ranging from 1 to 145. As for the square-lattice strip with $L = 7$, we have been unable to compute symbolically the characteristic polynomial of some of these blocks. Thus, the computation of the chromatic polynomial for finite strips of width $L = 7$ is beyond our computer facilities. However, as we can compute the eigenvalues and we know the amplitudes, we have been able to obtain the limiting curve.

In Figure 7(c) we show the zeros for a triangular-lattice strip of size $7_{\rm F} \times 7_{\rm P}$ (obtained using Eq. (2.18) and previous results for cylindrical boundary conditions [24]). We also show the limiting curve $\mathcal{B}$; it has been computed using the direct-search method. The same observations as for the square lattice with $L = 7$ hold in this case.

The limiting curve $\mathcal{B}$ crosses the real q-axis at $q = 0, 2, 3, B_8$ and $q = q_0 \approx 3.4682618071$. This is the first case for which we find five different "phases" on the real q-axis. We have found 12 T points at $q \approx 0.4951745217 \pm 2.1501328665\,i$, $q \approx 1.9229108754 \pm 2.4842273215\,i$, $q \approx 3.5014960312 \pm 0.2613477419\,i$, $q \approx 3.6121905140 \pm 1.1057902185\,i$, $q \approx 3.6937370146 \pm 0.8598201628\,i$, and $q \approx 3.8081077493 \pm 0.7447122915\,i$. As for the $L = 6$ case, we find two complex-conjugate endpoints at $q \approx 0.3195792189 \pm 1.8836441569$.[20] There are 3 isolated limiting points at $q = 1$, $q = B_5$, and $q = B_7$, as the value of q_0 is smaller than B_9.

5.7 $L = 8$

The full transfer matrix $\mathsf{T}(8)$ has dimension 424206, and can be split into 1500 blocks (see Table 3). We have computed the relevant nine blocks T_{ℓ,ℓ,j_0} from which all distinct eigenvalues can be obtained. As for $L = 7$, several of these blocks have large dimensions (up to 385). Thus, we have been unable to obtain the symbolic form of their characteristic polynomial. We can nevertheless compute the numerical values of the corresponding eigenvalues, and thus the limiting curve $\mathcal{B}$. The computation of this curve is very time consuming, whence we have focused on obtaining the point q_0 with great precision. Our result is $q_0 \approx 3.5134782609$. As this value is greater than B_8, we can observe a "phase" characterized by $\ell = 4$ bridges.

[19] Unfortunately we have been unable to use the resultant method to verify the existence of these endpoints. Instead, we have used the direct-search method to locate them. The endpoint character of these points is suggested by the following observation. If λ_1 and λ_2 are two (equimodular) dominant eigenvalues, we can define the (real) parameter $t = \tan(\theta/2)$, where θ is given by $\lambda_1/\lambda_2 = e^{i\theta}$ (see [22, Section 4.1.1]). Then, an endpoint is characterized by $t = 0$. At the points $q \approx 0.5716823545 \pm 1.9896139773\,i$, we have found that $t \approx 1.8 \times 10^{-6}$. This computation strongly suggest that these points are indeed endpoints.

[20] In this case, the parameter $t = \tan(\theta/2)$ (with θ given by $\lambda_1/\lambda_2 = e^{i\theta}$) takes the value $t \approx 3.2 \times 10^{-6}$. This small value suggests that these points are indeed endpoints.

Finally, we expect 3 isolated limiting points at $q = 1$, $q = B_5$, and $q = B_7$, as the value of q_0 is smaller than B_9.

6 Discussion

We have empirically found an interesting structure of the eigenvalues and amplitudes of the transfer matrix in terms of the number of bridges of the connectivity states ℓ. First, the transfer matrix has a lower-triangular block form (2.19). The blocks on the diagonal $T_{\ell,\ell}$ in turn have a diagonal block form (2.20) in terms of the sub-blocks $T_{\ell,\ell,j}$. The sub-blocks $T_{\ell,\ell,j}$ are characterized by the bottom-row connectivity state and the number ℓ and position of the bridges (modulo reflection symmetry with respect to the center of the strip for the square-lattice case). Second, all the eigenvalues of the transfer matrix can be obtained by diagonalizing, for each ℓ, only the largest of the sub-blocks. The final set of distinct eigenvalues can be then split into disjoint classes labeled solely by the number of bridges ℓ (i.e., if a given eigenvalue appears in several sub-blocks, all of these sub-blocks belong to block $T_{\ell,\ell}$ with ℓ bridges). Finally, all the eigenvalues belonging to the class of ℓ bridges have the common amplitude $\alpha^{(\ell)}$.

6.1 Phase diagram

Motivated by this structure we have tried to give a topological meaning to the closed regions into which the limiting curve divides the complex q-plane. In other words, in each region of the q-plane we want to know to which block $T_{\ell,\ell}$ the dominant eigenvalue belongs.

We first discuss the regions having a non-empty intersection I with the real q-axis. We invariably find that:

A. I is a simple interval in $\mathbb{R}^* \equiv \mathbb{R} \cup \{\infty\}$, which is either $I_n \equiv (B_{2n}, B_{2n+2})$ for $n = 1, 2, \ldots, n_{\max} - 1$, where $n_{\max}$ is determined by $B_{2n_{\max}} \le q_0(L) < B_{2n_{\max}+2}$, or $I_{n_{\max}} \equiv (B_{2n_{\max}}, q_0(L))$, or $I_0 \equiv \mathbb{R}^* \setminus [0, q_0(L)]$.

B. In the region containing I_n, with $n = 0, 1, \ldots, n_{\max}$, the dominant eigenvalue comes from the block with $\ell = n$ bridges. Its amplitude is thus $\alpha^{(n)}$.

We have verified the Properties A–B above for all the cyclic strips of the square and triangular lattices considered in Sections 3 and 5. We conjecture that they hold true for any strip width L, for the appropriate value of $q_0(L)$, and in the thermodynamic limit with $q_0(L)$ replaced by q_0. [For a discussion on the values of q_0, see the Introduction. See also Figures 8–9 for plots of the limiting curves $\mathcal{B}_L$ with $2 \le L \le 7$.]

In Ref. [26] a field theoretical mechanism was exhibited according to which the special role of the Beraha numbers in the case of *free* boundary conditions actually applies to the whole BK phase. We therefore finally conjecture that Properties A–B above hold within the entire BK phase, with $q_0(L)$ replaced by the boundary of the BK phase (in finite size, or in the $L \to \infty$ limit). [For the extent of the BK phase in the thermodynamic limit, see the Introduction].

Property B should be compared with Saleur's study of the square-lattice Potts model along the curve $v = -\sqrt{q}$, with $0 < q < 4$, i.e., the so-called unphysical self-dual line. In this

case one has $n_{\max} = \infty$, and it can be proved that the dominant eigenvalue for $q \in I_n$ indeed occurs in the spin n sector [26]. By renormalization group arguments one would expect this to extend to the entire BK phase. Another argument, asymptotically valid for $L \to \infty$, is that for $q \in I_n$ the effective central charge is maximal in the n-bridge sector (see below).

As to the regions inside the limiting curve that have an empty intersection with the real q-axis, we have found that in most cases (with $3 \le L \le 7$) the dominant eigenvalue corresponds to the class $\ell = 1$. There are however some exceptions to this rule:

- For the square lattice: For $L = 7$, the eigenvalues which are dominant inside the four tiny closed regions around $q \approx 2.71 \pm 0.85$ are characterized by either $\ell = 0$ or $\ell = 2$.
- For the triangular lattice: For $L = 5$, the tiny bulb-like regions emerging from T points at $q \approx 1.0114299869 \pm 2.1132511328\,i$, are characterized by $\ell = 2$ (note that those regions are completely surrounded by an $\ell = 1$ phase). Furthermore, the two small triangular-shaped regions around $q \approx 2.60 \pm 2.00\,i$ are characterized by $\ell = 0$. For $L = 6$, the two bulb-like regions emerging from T points at $q \approx 3.6870064797 \pm 0.810061005\,i$ are characterized by $\ell = 0$.

Therefore, we find that most of the limiting curves $\mathcal{B}$ corresponds to crossings (in modulus) of dominant eigenvalues coming from *different* blocks $T_{\ell,\ell}$. However, there are some exceptions to this general rule: we have found (in most cases, small) parts of $\mathcal{B}$ that correspond to crossings of dominant eigenvalues coming from the *same* block. For instance, the limiting curve for the square-lattice strip of width $L = 2$ contains a vertical segment which corresponds to crossings of two eigenvalues belonging to the $\ell = 1$ block. Smaller arcs with the same origin are also found for square-lattice strips with $L \le 3$ (except $L = 6$), and for triangular-lattice strips with $L \ge 5$.

6.2 Free energy and central charge

In order to gain further insight into the phase diagram we have computed the free energy per spin $f_L(q) = \frac{1}{L} \log \lambda_\star(q)$ for real q for strips of width L and infinite length, where $\lambda_\star$ denotes the dominant eigenvalue of the transfer matrix.

For $L \le 8$ this was done using the symbolic technique described in Sections 2–5. Another technique enabled us to extend these results to the range $L \le 11$. It consists in numerically diagonalizing the transfer matrix for a strip with fully free boundary conditions, but imposing the constraint that ℓ disjoint clusters propagate along the transfer direction. For each q, $\lambda_\star(q)$ was selected as the numerically largest among the $L+1$ eigenvalues which are dominant with respect to each possible ℓ-sector ($\ell = 0, 1, \ldots, L$). We have verified that for $L \le 8$ the two techniques give identical results.

In Figure 10(a) [resp. (b)] we plot $f_L(q)$ as a function of q for square-lattice (resp. triangular-lattice) strips with $2 \le L \le 11$ (resp. $2 \le L \le 10$). It is also useful to use instead of q, the (real) parameter n defined by

$$q \;=\; 4 \cos\left(\frac{\pi}{n}\right)^2 , \qquad n \ge 2 \,. \tag{6.1}$$

Special behavior (phase transitions, vanishing amplitudes, level crossings) is expected when n takes rational values. This is due to the special form (2.28) of the amplitudes $\alpha^{(\ell)}$, and to

the particularities of the representation theory of $\mathrm{U}_{\bar{q}}\,\mathrm{sl}(2)$ when $\bar{q}$ is a root of unity [25, 26]. The vertical dashed lines in Figures 10–13 correspond to even Beraha numbers $q = B_{2n}$.

For a critical system, conformal field theory predicts the following finite-size scaling behavior with free transverse boundary conditions [48, 49]:[21]

$$f_L(q) \;=\; f_{\mathrm{bulk}}(q) + \frac{f_{\mathrm{surf}}(q)}{L} + \frac{\pi G c(q)}{24 L^2} + o\bigl(L^{-2}\bigr)\,, \tag{6.2}$$

where $f_{\mathrm{bulk}}(q)$ and $f_{\mathrm{surf}}(q)$ are respectively the bulk and surface contributions to the free energy in the thermodynamic limit, $c(q)$ is the central charge, and the geometrical factor $G = 1$ (resp. $G = 2/\sqrt{3}$) for the square (resp. triangular [50]) lattice.[22] Neglecting all higher-order corrections on the right-hand side, one can obtain approximations to $f_{\mathrm{bulk}}(q)$, $f_{\mathrm{surf}}(q)$, and $c(q)$ from fits involving three system sizes: $L = L_{\mathrm{min}}, L_{\mathrm{min}}+1, L_{\mathrm{min}}+2$. However, we find that the $o(L^{-2})$ terms are important and our estimates for $c(q)$ have strong finite-size-scaling effects.

In order to obtain accurate estimators for $c(q)$ we need to include the first correction-to-scaling terms in (6.2). We have used the following improved Ansatz:

$$f_L(q) \;=\; f_{\mathrm{bulk}}(q) + \frac{f_{\mathrm{surf}}(q)}{L} + \frac{\pi G c(q)}{24 L^2} + \frac{A}{L^3} + \frac{B}{L^4}\,. \tag{6.3}$$

The L^{-3} term is the expected (non-universal) contribution of the non-singular part of the free energy due to the free transverse boundary conditions (see e.g., the discussion in Privman's review [51]). The last L^{-4} term is a non-universal correction predicted by conformal field theory.[23]

We have obtained approximations to $f_{\mathrm{bulk}}(q)$, $f_{\mathrm{surf}}(q)$, and $c(q)$ from fits involving five system sizes: $L = L_{\mathrm{min}} + k$ with $0 \le k \le 4$. The best approximations for $f_{\mathrm{bulk}}(q)$, with $L_{\mathrm{min}} = 7$ (resp. $L_{\mathrm{min}} = 6$) for the square (resp. triangular) lattice, are displayed as (black) solid circles in Figure 10. The corresponding estimates for $c(q)$ are shown in Figure 11, and for $f_{\mathrm{surf}}(q)$ in Figure 12. Finally, for the triangular lattice we have also tried a four-parameter Ansatz, obtained from (6.3) by fixing $f_{\mathrm{bulk}}(q)$ to its analytically known value [21]. The resulting estimates for $f_{\mathrm{surf}}(q)$ and $c(q)$ are shown in Figure 13.

The estimates for the bulk free energy $f_{\mathrm{bulk}}(q)$ shown in Figure 10 are rather smooth as a function of q, except close to q_0. In the triangular-lattice case (b), we have also shown the exact value of $f_{\mathrm{bulk}}(q)$ with *cylindrical* boundary conditions, as obtained by Baxter [21]. The very good agreement supports the idea that $f_{\mathrm{bulk}}(q)$ is independent of (reasonable) boundary conditions. However, for $q \approx q_0$ this agreement is not longer good, due to large correction-to-scaling effects. In particular, for the triangular lattice our numerical results for $3.5 \lesssim q \lesssim 4$

[21] Formula (6.2) is valid for two-dimensional systems only for manifolds with Euler number $\chi = 0$ [49]. If $\chi \neq 0$, then an additional term $\sim L^{-2} \log L$ appears [49].

[22] Note that $f_L(q)$ is the free energy per spin, whereas the standard CFT formulae require normalization per unit area. To redraw Figure 5 in an undistorted way (i.e., with each triangular plaquette being equilateral) the time slices must make an angle $\alpha = 2\pi/3$ with the transfer direction. The projected width of an L-spin strip is thus $L \sin\alpha = L/G$ lattice spacings.

[23] There are indeed many more non-universal corrections terms due to irrelevant operators and some of them might be more relevant than the L^{-4} term included in the Ansatz (6.3). However, we expect that the L^{-4} term can mimic the effect of such higher-order terms.

do not shed light on the question of which of Baxter's eigenvalues is dominant where, and hence on the value of q_0(tri) (See [24] for a more comprehensive discussion on this issue).

The results for $c(q)$ make sense within the critical BK phase, i.e., for $0 < q < q_0$, where $q_0(\mathrm{sq}) = 3$ and $q_0(\mathrm{tri}) = 2 + \sqrt{3}$ (but see the Introduction for a discussion of the latter value). Estimates for both lattice types, and for different values of $2 \leq L_{\min} \leq 7$, are displayed in Figure 11. The variation with respect to $L_{\min}$ is a measure of the size of the residual corrections to scaling.

It should be noted that the effective central charge c_{eff} (i.e., the one observed on the above plots) depends on both the "real" central charge c_{real} (i.e., the one computed from field theory) and the critical exponents $\tilde{x}_\ell$ corresponding to the insertion of ℓ bridges. The latter are actually surface critical exponents, since the transverse boundary conditions are free. We have for the BK phase [52]

$$c_{\mathrm{real}} = 1 - \frac{6(n-1)^2}{n} \tag{6.4}$$

$$\tilde{x}_\ell = \frac{\ell^2 - (n-1)\ell}{n} \tag{6.5}$$

and since $\ell = \lfloor n/2 \rfloor$ from Property A of Section 6.1, we find

$$c_{\mathrm{eff}}(q) = c - 24\tilde{x}_\ell = 1 - 6\frac{(n-1)^2 - 4\left(\lfloor \frac{n}{2} \rfloor^2 - (n-1)\lfloor \frac{n}{2} \rfloor\right)}{n} . \tag{6.6}$$

This continuous oscillatory function is shown in Figures 11 and 13(b). Note that for n an even integer one has $c_{\mathrm{eff}} = 1 - 6/n$, while for n an odd integer one has $c_{\mathrm{eff}} = 1$ independently of n. However, exactly for integer n we do not expect (6.6) to hold (see below). Note that for free longitudinal boundary conditions by contrast, only the $\ell = 0$ sector contributes, and thus the effective central charge (6.6) is equal to the BK value (6.4).

Finally, for values of q outside the limiting curve we generally find that the effective central charge is close to zero, consistent with non-critical behavior. Indeed, with a finite bulk correlation length ξ, the scaling form (6.3) must be replaced by

$$f_L(q) = f_{\mathrm{bulk}}(q) + \frac{f_{\mathrm{surf}}(q)}{L} + O\left(e^{-L/\xi}\right) . \tag{6.7}$$

Note however that for the triangular lattice, we expect the regime $q_0(\mathrm{tri}) < q \leq 4$ to be critical [54, 52]. In particular the case $q = 4$ is equivalent to the three-coloring of the bonds of the hexagonal lattice [53], a critical model with $c = 2$ [55]. In addition, the 3-state zero-temperature square-lattice Potts antiferromagnetic model can be mapped to the F-model (*alias* the equal-weighted six-vertex model) [56, 57], which is a critical $c = 1$ theory.

In the case of the triangular lattice, we have also tried a four-parameter Ansatz, obtained from (6.3) by fixing $f_{\mathrm{bulk}}(q)$ to its analytically known value [21]. In Figure 13(a) we have plotted the corresponding estimates for $f_{\mathrm{surf}}(q)$, and in Figure 13(b) the estimates for the central charge. While we find a smooth behavior of $f_{\mathrm{surf}}(q)$ for $q \lesssim 3$ and $q \gtrsim 4$, there is a rather abrupt behavior in the regime $3 \lesssim q \lesssim 4$. In that region we should expect strong finite-size-scaling corrections due to the proximity of several phase transitions. We conjecture that $f_{\mathrm{surf}}(q)$ has a jump discontinuity at $q = q_0$, while $f_{\mathrm{bulk}}(q)$ is a continuous function of q (Baxter [21] explicitly showed that $f_{\mathrm{bulk}}(q)$ is continuous for the triangular lattice).

Our best numerical results for the central charge contained in Figures 11(a) (square lattice) and 13(b) (triangular lattice), show a remarkable agreement with the theoretical prediction for $c_{\rm eff}(q)$ (6.6) in the interval $q \in (0,2)$. We also find good agreement with the prediction $c = 0$ in the non-critical region for $q \lesssim -0.4$, and $q \gtrsim 3.5$ (resp. $q \gtrsim 4.5$) for the square (resp. triangular) lattice. For $q \lesssim 0$ and $q \gtrsim q_0$ there are strong corrections to scaling because the central charge is discontinuous at those points. Finally, we remark that at $q = q_0$ we find excellent agreement with the theoretical predictions: $c = 1.00(1)$ for the $q = 3$ model on the square lattice, and $c = 2.01(5)$ for the $q = 4$ model on the triangular lattice.[24]

6.3 Isolated limiting points and real crossings of the limiting curve

We recall that isolated limiting points occur when the amplitude of the dominant eigenvalue vanishes. In Tables 5 and 6 we show the real chromatic zeros for strips of size $L_{\rm F} \times (kL)_{\rm P}$ with $1 \le k \le 10$. As explained in Ref. [22], the convergence to isolated limiting points is exponentially fast.

First note that $\alpha^{(0)} = 1$ never vanishes. Concerning the region containing I_n (with $n = 1, 2, \ldots, n_{\max}$), we remark that as q moves through the interval $[B_{2n}, B_{2n+2}]$, $\alpha^{(n)}$ increases monotonically from -1 to 1, passing through 0 when $q = B_{2n+1}$. (This statement can be easily proved from the first of the definitions in (2.26).) In conjunction with the fact that all zeros of the Chebyshev polynomials of the second kind are real, the Properties A–B of Section 6.1 give the corollary:

- An isolated limiting point must necessarily be real.
- No isolated limiting point exists in the region containing I_0. For $n = 1, 2, \ldots, n_{\max} - 1$, the region containing I_n has exactly one isolated limiting point which is B_{2n+1}. The region containing $I_{n_{\max}}$ has the isolated limiting point $B_{2n_{\max}+1}$ provided that $B_{2n_{\max}+1} < q_0(L)$.

As before, we conjecture the validity of these properties for any L, and for the entire BK phase.

By definition, the limiting curve crosses the real q-axis in $q_0(L)$. Further crossings are possible for $0 \le q < q_0(L)$, provided that the two dominant eigenvalues become degenerate and that the corresponding amplitudes differ only by a sign. From (2.26) it is easy to see that the last condition is satisfied for $q = B_{2n}$ with $n = 1, 2, \ldots, n_{\max}$. That the first condition is also satisfied follows from the $\mathrm{U}_{\bar{q}}\,\mathrm{sl}(2)$ symmetry [26], and we have also verified this directly for all strips studied in this paper.

In the thermodynamic limit we have $q_0(\mathrm{sq}) = 3$ and $q_0(\mathrm{tri}) = B_{12} = 2 + \sqrt{3}$ (as discussed in the Introduction). For the square lattice chromatic polynomial, we thus predict that the limiting curve crosses the real q-axis three times (at B_2, B_4 and B_6), dividing the real q-axis into three different phases (corresponding to $\ell = 0, 1, 2$). Furthermore, there are two isolated

[24] At $q = q_0$ we find that the dominant sector is $\ell = 0$, thus there are no corrections due to the exponents $\widetilde{x}_\ell$ (6.5). In addition, when performing the fits close to $q = 4$ for the triangular lattice (with the exact value of $f_{\rm bulk}(q)$), we have found noticeable even–odd oscillations. The estimate $c = 2.01(5)$ for $q = 4$ has been obtained by fitting data points with $L = 4, 6, 8, 10$.

limiting points (at B_3 and B_5). For the triangular lattice, the limiting curve crosses the real q-axis seven times (at $B_2, B_4, \ldots, B_{12}$, and at B_∞), dividing the real q-axis into seven different phases (corresponding to $\ell = 0, \ldots, 6$). Furthermore, there are five isolated limiting points (at $B_3, B_5, \ldots, B_{11}$).

6.4 Cancellations for $q = B_n$, n integer

One important point about the BK phase is that it is *not* defined for $q = B_n$ with n integer [26]. In these cases there are cancellations among eigenvalues that give rise to a different physics.

The most trivial case corresponds to $q = B_2 = 0$. At this value the coefficients $\alpha^{(\ell)}$ (2.25) take the form

$$\alpha^{(\ell)}(q=0) \;=\; \begin{cases} 1 & \text{if } \mathrm{mod}(\ell,2) = 0 \\ -1 & \text{otherwise} \end{cases} \tag{6.8}$$

We have seen that the eigenvalues become degenerate in pairs, one belonging to an odd-ℓ sector, and the other one to an even-ℓ sector. Thus there is a complete cancellation of all eigenvalues and the result is as expected, $Z_{G_n}(0) = 0$.

At $q = B_3 = 1$, the coefficients take the form

$$\alpha^{(\ell)}(q=1) \;=\; \begin{cases} 1 & \text{if } \mathrm{mod}(\ell,3) = 0 \\ 0 & \text{if } \mathrm{mod}(\ell,3) = 1 \\ -1 & \text{if } \mathrm{mod}(\ell,3) = 2 \end{cases} \tag{6.9}$$

The (non-zero) eigenvalues with non-zero amplitudes become degenerate forming $2n$-tuples. Exactly n of them have $\alpha = 1$, and the other half, $\alpha = -1$. Thus, there is an exact cancellation of all contributions, giving $Z_{G_n}(q=1) = 0$.

For $q = B_4 = 2$, the coefficients take the form

$$\alpha^{(\ell)}(q=2) \;=\; \begin{cases} 1 & \text{if } \mathrm{mod}(\lfloor \ell/2 \rfloor,2) = 0 \\ -1 & \text{otherwise} \end{cases} \tag{6.10}$$

In the triangular-lattice case we find a similar cancellation as for the $q = 1$ case: the non-zero eigenvalues with non-zero amplitude form $2n$-tuples whose net contribution is zero. Thus, in this case we also have the expected result $Z_{G_n}(q=2) = 0$. For the square lattice we find a non-critical behavior: there is an exact cancellation of all non-zero eigenvalues, except for those taking values $\lambda = \pm 1$. The net contribution for a $L \times n$ lattice is always of the form $Z_{L\times n} = 2$ if n is even, and $Z_{L\times n} = 0$ if n is odd.

The last trivial case corresponds to $q = B_6 = 3$ for the triangular lattice. This is very similar to $q = 2$ for the square lattice: all non-zero eigenvalues cancel exactly, except those with $\lambda = \pm 1$. Again, for each triangular lattice of size $L \times n$ the net contribution is given by $Z_{L\times n} = 6$ if $\mathrm{mod}(n,3) = 0$, and $Z_{L\times n} = 0$ otherwise.

For the square lattice the only non-trivial case is $q = B_5$.[25] Up to $L = 5$ we find that the dominant eigenvalue (belonging to the $\ell = 0$ sector) actually contributes to the partition

[25]The value $q = B_6 = 3$ is also non-trivial, as we expect a critical point for the 3-state antiferromagnet at zero temperature. However, we have found that the dominant eigenvalue (for all widths $L \leq 8$) belongs to the $\ell = 0$ sector, and $\alpha^{(0)} \neq 0$.

function. But for $6 \le L \le 8$, we find that the dominant eigenvalue belongs to the $\ell = 2$ sector, and $\alpha^{(2)}(q = B_5) = 0$. The first non-zero contribution corresponds to a singlet belonging to $\lambda = 0$. The numerical results are given in Table 8.

For the triangular lattice, the value $q = B_5$ is also non-trivial. The dominant eigenvalue belongs to the $\ell = 2$ sector, but again $\alpha^{(2)}(q = B_5) = 0$. In this case, as L increases the first eigenvalue contributing to the partition function is deeper into the spectrum of the transfer matrix. For even L, this eigenvalue is complex and belongs to $\ell = 1$, and for odd L, it is real and belongs to $\ell = 0$. See Table 8 for the numerical results.

For $q = B_7$, the dominant eigenvalue has $\ell = 0$ for $2 \le L \le 4$, and $\ell = 3$ for $5 \le L \le 8$. This latter case is the interesting one, as the corresponding amplitude vanishes. We find that the first eigenvalue that gives a net contribution to the partition function belongs to $\ell = 0$, and as L increases, its position in the transfer-matrix spectrum lowers rapidly. See Table 8 for the numerical results.

These results show that exactly at $q = B_n$ the physics of the system is not described by the BK phase. In some cases $q = 0, 1, 2$ (and $q = 3$ for the triangular lattice) the partition function is trivial. In other cases, $q = B_5$ and $q = B_7$ (the latter one only for the triangular lattice), the free energy comes from a subdominant eigenvalue of the transfer matrix. We refrain from extracting the effective central charge from the results displayed in Table 8; as the data shows strong parity effects and the number of data points is rather limited.

A Alternative construction of the transfer matrix for square-lattice strips with cyclic boundary conditions

We have already discussed in Section 2 how to build the transfer matrix for a square-lattice strip with cyclic boundary conditions: the idea was to leave the bottom row fixed and act only on the top row. This procedure leads to fairly large transfer matrices with a block structure. Each block is labeled by the bottom-row connectivity and the number and position of the bridges joining the top and bottom rows (modulo reflection symmetry) This transfer matrix is *not* invariant under the operation of interchanging the top and bottom rows. This latter operation can be viewed as a reflection with respect to the middle of the strip (in the longitudinal direction). For simplicity, we will call it a t-reflection.

Smaller transfer matrices invariant under t-reflections can be built as follows. The idea is to obtain a transfer matrix acting on both the top and bottom rims. Thus, the matrices H and V take the form

$$\widehat{\mathsf{H}}(m) \;=\; \prod_{i=1}^{m-1} \mathsf{Q}_{i,i+1} \cdot \prod_{i=1}^{m-1} \mathsf{Q}_{i',(i+1)'} \tag{A.1a}$$

$$\widehat{\mathsf{V}}(m) \;=\; \prod_{i=1}^{m} \mathsf{P}_{i} \cdot \prod_{i=1}^{m} \mathsf{P}_{i'} \cdot \tag{A.1b}$$

These two matrices act on the top and bottom rows simultaneously, and are by construction t-invariant (i.e. invariant under a t-reflection $i \leftrightarrow i'$). The t-invariant transfer matrix is defined as

$$\widehat{\mathsf{T}}(m) \;=\; \widehat{\mathsf{V}}(m) \cdot \widehat{\mathsf{H}}(m) \; . \tag{A.2}$$

Note that as we are acting on both rims simultaneously, we can only obtain the partition function for strips of even length. Then, the partition function for a square-lattice strip of size $m \times 2n$ is given by

$$P_{m\times 2n}(q) \;=\; \boldsymbol{u}^{\mathrm{T}} \cdot \widehat{\mathsf{H}}(m) \cdot \widehat{\mathsf{T}}(m)^n \cdot \boldsymbol{v}_{\mathrm{id}} \tag{A.3}$$

where the matrices $\widehat{\mathsf{H}}$ and $\widehat{\mathsf{T}}$ are given by (A.1a)/(A.2).

As we are considering the chromatic–polynomial case, the matrix $\widehat{\mathsf{H}}$ is a projector, and then it is more convenient to use the modified transfer matrix (see Section 2)

$$\widehat{\mathsf{T}}'(m) \;=\; \widehat{\mathsf{H}}(m) \cdot \widehat{\mathsf{V}}(m) \cdot \widehat{\mathsf{H}}(m) \tag{A.4}$$

and the connectivity-state basis

$$\boldsymbol{w}_{\mathcal{P}} \;=\; \widehat{\mathsf{H}}(m) \cdot \boldsymbol{v}_{\mathcal{P}} \tag{A.5}$$

As in Section 2, we will consider hereafter this modified transfer matrix with the prime dropped.

The fact the transfer matrix (A.2) is now t-invariant can be used to obtain a smaller transfer matrix. We can pass to a new basis consisting on connectivities that are either even or odd under t-reflection.[26] In this new basis the transfer matrix takes the block-diagonal form

$$\widehat{\mathsf{T}}(m) \;=\; \begin{pmatrix} \widehat{\mathsf{T}}_+(m) & 0 \\ 0 & \widehat{\mathsf{T}}_-(m) \end{pmatrix} \tag{A.6}$$

where $\widehat{\mathsf{T}}_+$ (resp. $\widehat{\mathsf{T}}_-$) corresponds to the subspace which is even (resp. odd) under a t-reflection. The left and right vectors take the form

$$\boldsymbol{w}_{\mathrm{id}}^T \;=\; \left(\boldsymbol{w}_{\mathrm{id},+}^T, 0\right) \tag{A.7a}$$

$$\boldsymbol{u}^T \;=\; \left(\boldsymbol{u}_+^T, 0\right) , \tag{A.7b}$$

as the start vector $\boldsymbol{w}_{\mathrm{id}}$ is clearly t-reflection invariant, and the action of $\boldsymbol{u}^T$ on any t-reflection-odd connectivity is identically zero. Thus, the contribution of the t-reflection-odd subspace to the partition function vanishes, and we can work entirely within the t-reflection-invariant subspace. The dimension of this subspace for a square-lattice of width m is denoted by SqRingT(m) in Table 9. We expect that for large enough width m, the dimension of the t-reflection-invariant subspace will be approximately one half of the original dimension.

This transfer matrix also has a block structure. In this case, due to its invariance under t-reflection, the blocks are labeled merely by the number of bridges ℓ joining the top and bottom rows. Thus, for a strip of width m, the transfer matrix $\widehat{\mathsf{T}}(m)$ can be split into $\ell = m+1$ blocks, as in eq. (2.19):

$$\widehat{\mathsf{T}}(m) \;=\; \begin{pmatrix} \widehat{T}_{m,m} & 0 & \dots & 0 \\ \widehat{T}_{m-1,m} & \widehat{T}_{m-1,m-1} & \dots & 0 \\ \vdots & \vdots & & \vdots \\ \widehat{T}_{0,m} & \widehat{T}_{0,m-1} & \dots & \widehat{T}_{0,0} \end{pmatrix} \tag{A.8}$$

[26] Let us denote $\{\boldsymbol{v}_i\}$ the connectivity basis. Some of these elements are t-invariant; the rest can be grouped into pairs $(\boldsymbol{v}_a, \boldsymbol{v}_b)$ that map into each other under a t-reflection. A basis for the even (i.e., t-reflection invariant) subspace is then given by the elements of the first set together with the combinations $\boldsymbol{v}_a + \boldsymbol{v}_b$ from the second set. A basis for the odd subspace is given by the combinations $\boldsymbol{v}_a - \boldsymbol{v}_b$ from the second set.

The difference with the method discussed in Section 2 is that now each diagonal block $\widehat{T}_{\ell,\ell}$ does not have in general any sub-block structure, like in 2.20. The dimension of the largest block of $\widehat{\mathsf{T}}$ is in general greater than the dimension of the largest block of T (see Tables 9 and 2). As an example, for width $m = 5$, the largest block of the matrix $\mathsf{T}(5)$ has dimension 21; but the dimension of the largest block of $\widehat{\mathsf{T}}(5)$ is 127. The fact that the dimension of the largest block for $\widehat{\mathsf{T}}$ grows very quickly with the strip width, makes the symbolic computation of its characteristic polynomial (and hence, of its eigenvalues) a difficult task.

The simplest case is the strip of width $m = 2$. The basis (3.2) we used to construct the matrix $\mathsf{T}(2)$ is already t-reflection invariant. In this basis, the matrix $\widehat{\mathsf{T}}(2)$ takes the form

$$\widehat{\mathsf{T}}(2) \;=\; \left(\begin{array}{c|cc|c} 1 & 0 & 0 & 0 \\ \hline q-3 & q^2-4q+5 & 4-2q & 0 \\ -1 & 4-2q & q^2-4q+5 & 0 \\ \hline q^2-5q+8 & T_{42} & T_{42} & (q^2-3q+3)^2 \end{array}\right) \tag{A.9}$$

with

$$T_{42} \;=\; 2(q-2)(q^2-4q+6) \tag{A.10}$$

The right $\boldsymbol{w}_{\rm id}$ and left $\boldsymbol{u}$ vectors are equal to those given by (3.3). It is easy to verify that

$$\widehat{\mathsf{T}}(2) \;=\; \mathsf{T}(2)^2 \tag{A.11}$$

This result is expected as both matrices are written in the same basis and each time we act with $\widehat{\mathsf{T}}(2)$ we add two layers to the strip.

The first non-trivial case corresponds to the strip of width $m = 3$. In this case the t-reflection-invariant basis has dimension 15. We have found four blocks labeled by the number of bridges ℓ:

- $\ell = 3$: This block is one-dimensional and the eigenvalue is $\lambda = 1$.
- $\ell = 2$: This block is four-dimensional and the eigenvalues are $\lambda = (q-4)^2, (q-1)(q-4), (q-2)^2$, and $(q-1)^2$.
- $\ell = 1$: This block has dimension 10. One eigenvalue is $\lambda = (q-1)(q^3-6q^2+13q-11)$ and the other ones come from solving two different equations of third order.
- $\ell = 0$: This block is three-dimensional. One eigenvalue is $\lambda = (q-2)^4$ and the other two are the solutions of a second-order equation.

Thus, we find 15 distinct eigenvalues. This number is larger than the number of distinct eigenvalues for this strip (see eq. (3.8)). Indeed, we have verified that the amplitudes corresponding to five of the above eigenvalues are identically zero. As a matter of fact, the zero amplitudes correspond to the eigenvalues that are not positive definite for real q (e.g., $\lambda = (q-1)(q-4)$ and $(q-1)(q^3-6q^2+13q-11)$). This is expected as the transfer matrix $\widehat{\mathsf{T}}$ is physically equivalent to T^2: hence, the former must contain the square of the eigenvalues of the latter.

We have checked that this procedure works also for the square-lattice strip of width $m = 4$ and the result agrees with the one presented in the text.

Remark: This procedure can also be implemented for the triangular lattice. In this case, the relevant symmetry is a t-reflection followed by a (standard) reflection with respect to the center of the strip. This second step is needed to bring the diagonal bonds into the right position.

Acknowledgments

We wish to thank Jean–François Richard for some interesting comments on an earlier version of this paper, Hubert Saleur for sharing his insight in quantum groups, and Alan Sokal for discussions and his collaborations on related projects. We also thank an anonymous referee for many useful suggestions that improved the presentation of our results. This research was partially supported by U.S. National Science Foundation grant PHY-0116590 and by CICyT (Spain) grant MTM2004-01728 (J.S.).

References

[1] P.W. Kasteleyn and C.M. Fortuin, J. Phys. Soc. Japan **26** (Suppl.), 11 (1969); C.M. Fortuin and P.W. Kasteleyn, Physica **57**, 536 (1972).

[2] V. Pasquier, J. Phys. A **20**, L1229 (1987).

[3] G.E. Andrews, R.J. Baxter and P.J. Forrester, J. Stat. Phys. **35**, 193 (1984).

[4] D.A. Kurtze and M.E. Fisher, Phys. Rev. B **20**, 2785 (1979).

[5] Y. Shapir, J. Phys. A **15**, L433 (1982).

[6] D. Dhar, Phys. Rev. Lett. **51**, 853 (1983).

[7] D. Poland, J. Stat. Phys. **35**, 341 (1984).

[8] A. Baram and M. Luban, Phys. Rev. A **36**, 760 (1987).

[9] A.J. Guttmann, J. Phys. A **20**, 511 (1987).

[10] S.-N. Lai and M.E. Fisher, J. Chem. Phys. **103**, 8144 (1995).

[11] Y. Park and M.E. Fisher, Phys. Rev. E **60**, 6323 (1999), cond-mat/9907429.

[12] S. Todo, Int. J. Mod. Phys C **10**, 517 (1999), cond-mat/9703176.

[13] D.C. Brydges and J.Z. Imbrie, Ann. Math. **158**, 1019 (2003), math-ph/0107005; J. Stat. Phys. **110**, 503 (2003), math-ph/0203055.

[14] C.N. Yang and T.D. Lee, Phys. Rev. **87**, 404 (1952). T.D. Lee and C.N. Yang, *ibid.* **87**, 410 (1952).

[15] P.J. Kortman and R.B. Griffiths, Phys. Rev. Lett. **27**, 1439 (1971).

[16] M.E. Fisher, Phys. Rev. Lett. **40**, 1610 (1978).

[17] O.F. de Alcantara Bonfim, J.E. Kirkham and A.J. McKane, J. Phys. A **14**, 2391 (1981).

[18] G. Parisi and N. Sourlas, Phys. Rev. Lett. **46**, 871 (1981).

[19] J.L. Cardy, Phys. Rev. Lett. **54**, 1354 (1985).

[20] C. Itzykson, H. Saleur and J.-B. Zuber, Europhys. Lett. **2**, 91 (1986).

[21] R.J. Baxter, J. Phys. A **19**, 2821 (1986); *ibid.* **20**, 5241 (1987).

[22] J. Salas and A.D. Sokal, J. Stat. Phys. **104**, 609 (2001), cond-mat/0004330.

[23] J.L. Jacobsen and J. Salas, J. Stat. Phys. **104**, 701 (2001), cond-mat/0011456.

[24] J.L. Jacobsen, J. Salas, and A.D. Sokal, J. Stat. Phys. **112**, 921 (2003), cond-mat/0204587.

[25] V. Pasquier and H. Saleur, Nucl. Phys. B **330**, 523 (1990).

[26] H. Saleur, Commun. Math. Phys. **132**, 657 (1990); Nucl. Phys. B **360**, 219 (1991).

[27] R. J. Baxter, J. Phys. C **6**, L445 (1973).

[28] R.J. Baxter, *Exactly Solved Models in Statistical Mechanics* (Academic Press, London–New York, 1982).

[29] B. Nienhuis, in *Phase Transitions and Critical Phenomena*, Vol. 11, edited by C. Domb and J. L. Lebowitz (Academic, London, 1987).

[30] R.J. Baxter, Proc. Roy. Soc. London A **383**, 43 (1982).

[31] J.L. Jacobsen and H. Saleur, The antiferromagnetic Potts model, in preparation.

[32] R.J. Baxter, H.N.V. Temperley and S.E. Ashley, Proc. Roy. Soc. London A **358**, 535 (1978).

[33] J.L. Jacobsen, J. Salas and A.D. Sokal, J. Stat. Phys. **119**, 1153 (2005), cond-mat/0401026.

[34] S. Beraha, J. Kahane, and N.J. Weiss, Proc. Nat. Acad. Sci. USA **72**, 4209 (1975). For a slightly more general theorem and a complete list of references see A.D. Sokal, Combin. Probab. Comput. **13**, 221 (2004), cond-mat/0101197.

[35] N.L. Biggs, R.M. Damerell and D.A. Sands, J. Combin. Theory B **12**, 123 (1972).

[36] R. Shrock and S.-H. Tsai, Physica A **275**, 429 (2000), cond-mat/9907403.

[37] S.-C. Chang and R. Shrock, Physica A **290**, 402 (2001), cond-mat/0004161.

[38] S.-C. Chang and R. Shrock, Physica A **316**, 335 (2002), cond-mat/0201223.

[39] S.-C. Chang and R. Shrock, Ann. Phys. (N.Y.) **290**, 124 (2001), cond-mat/0004129.

[40] S.-C. Chang and R. Shrock, Physica A **347**, 314 (2005), cond-mat/0404524.

[41] S.-C. Chang and R. Shrock, Physica A **346**, 400 (2005), cond-mat/0404373.

[42] M. Noy and A. Ribó, Adv. Appl. Math. **32**, 350 (2004).

[43] S.-C. Chang and R. Shrock, Physica A **296**, 131 (2001), cond-mat/0005232.

[44] N.J.A. Sloane, Sloane's On-Line Encyclopedia of Integer Sequences, `http://www.research.att.com/~njas/sequences/index.html`

[45] I. Gradshtein and I. Ryzhik, Tables of Integrals, Series, and Products (Academic Press, New York, 1980).

[46] S.-C. Chang and R. Shrock, Physica A **347**, 314 (2005), cond-mat/0404524.

[47] D.R. Woodall, Discrete Math. **172**, 141 (1997).

[48] H.W.J. Blöte, J.L. Cardy and M.P. Nightingale, Phys. Rev. Lett. **56**, 742 (1986).

[49] J.L. Cardy and I. Peschel, Nucl. Phys. B **300**, 377 (1988).

[50] J.O. Indekeu, M.P. Nightingale, and W.V. Wang, Phys. Rev. B **34**, 330 (1986).

[51] V. Privman, in *Finite Size Scaling and Numerical Simulation of Statistical Physics*, pp. 1–98 (World Scientific, Singapore, 1990).

[52] B. Duplantier and H. Saleur, Nucl. Phys. B **290**, 291 (1987).

[53] R.J. Baxter, J. Math. Phys. **11**, 784 (1970).

[54] B. Nienhuis, Phys. Rev. Lett. **49**, 1062 (1982).

[55] M.T. Batchelor, J. Suzuki and C.M. Yung, Phys. Rev. Lett. **73**, 2646 (1994).

[56] A. Lenard, cited in E.H. Lieb, Phys. Rev. **162**, 162 (1967) at pp. 169-170.

[57] R.J. Baxter, J. Math. Phys. **11**, 3116 (1970).

m	C_{2m}	TriRing	SqRing	SqRing′
1	2	2	2	2
2	14	6	4	4
3	132	30	20	10
4	1430	178	94	26
5	16796	1158	614	70
6	208012	7986	4028	192
7	2674440	57346	28940	534
8	35357670	424206	212370	1500
9	477638700	3210246	1607246	4246
10	6564120420			12092

Table 1: Dimensionality of the transfer matrix for cyclic boundary conditions. For each square-lattice width m we give the number of non-crossing partitions C_{2m}, non-crossing non-nearest-neighbor partitions TriRing, the number of classes of partitions invariant under reflections SqRing, and the number of distinct eigenvalues SqRing′ [43].

m	N_0	N_1	N_2	N_3	N_4	N_5	N_6	N_7	N_8	N_9	# blocks
2	1	1	1								3
3	2	3	2	1							8
4	3	5	5	2	1						16
5	7	13	12	8	3	1					44
6	13	27	30	20	11	3	1				105
7	32	70	77	61	34	15	4	1			294
8	70	166	199	163	106	49	19	5	1		777
9	179	435	528	468	318	174	72	24	5	1	2204

Table 2: Block structure of the transfer matrix of a cyclic square-lattice strip of width m as a function of number of bridges ℓ. For each strip width m, we quote the number of blocks N_ℓ for a given number of bridges ℓ, and the total number of blocks (# blocks).

m	L_0	L_1	L_2	L_3	L_4	L_5	L_6	L_7	L_8	L_9	SqRing′
2	1	2	1								4
3	2	4	3	1							10
4	4	9	8	4	1						26
5	9	21	21	13	5	1					70
6	21	51	55	39	19	6	1				192
7	51	127	145	113	64	26	7	1			534
8	127	323	385	322	203	97	34	8	1		1500
9	323	835	1030	910	622	334	139	43	9	1	4246

Table 3: Block structure of the transfer matrix of cyclic square- and triangular-lattice strips of width m as a function of number of bridges ℓ. For each strip width m, we quote the number of different eigenvalues L_ℓ for a given number of bridges ℓ, and the total number of distinct eigenvalues SqRing′(m). For the triangular lattice, the number of blocks N_ℓ for a given value of ℓ coincide with the number of distinct eigenvalues L_ℓ for the same value of ℓ.

	Eigenvalue-Crossing Curves $\mathcal{B}$						Isolated Points
Lattice	# C	# E	# T	# D	# ER	q_0	# RI
$2_{\rm R}$	1	0	2	1	3	2	1
$3_{\rm R}$	1	0	10	0	6	2.3365442725	1
$4_{\rm R}$	1	0	6	0	4	2.4928455591	1
$5_{\rm R}$	$1^\dagger$	$0^\dagger$	$6^\dagger$	$0^\dagger$	$4^\dagger$	2.5823854661	1
$6_{\rm F}$	$1^\dagger$	$0^\dagger$	$10^\dagger$	$0^\dagger$	$6^\dagger$	2.6460783059	2
$7_{\rm F}$	$1^\dagger$	$0^\dagger$	$14^\dagger$	$0^\dagger$	$8^\dagger$	2.6927280047	2
$8_{\rm F}$						2.7287513178	2

Table 4: Summary of qualitative results for the square-lattice eigenvalue-crossing curves $\mathcal{B}$ and for the isolated limiting points of zeros. For each cyclic square-lattice strip considered in this paper, we give the number of connected components of $\mathcal{B}$ (# C), the number of endpoints (# E), the number of T points (# T), the number of double points (# D), and the number of enclosed regions (# ER). We also give the value q_0 which is the largest real value where $\mathcal{B}$ intersects the real axis, and the number of real isolated limiting points of zeros (# RI). The symbol † indicates uncertain results.

Lattice	3rd Zero	4th Zero
$3_F \times 3_P$	2	2.453397651516
$3_F \times 6_P$	2.055981832687	2.096994387849
$3_F \times 9_P$	2	
$3_F \times 12_P$	2.000122296702	2.293027675252
$3_F \times 15_P$	2	
$3_F \times 18_P$	2.000001089940	2.317707700956
$3_F \times 21_P$	2	
$3_F \times 24_P$	2.000000011921	2.325316414328
$3_F \times 27_P$	2	
$3_F \times 30_P$	2.000000000143	2.328289813540
$4_F \times 4_P$		
$4_F \times 8_P$	2.000043877962	2.370251603751
$4_F \times 12_P$	2.000000074707	2.430973630621
$4_F \times 16_P$	2.000000000188	2.453300957620
$4_F \times 20_P$	2.000000000001	2.464208849270
$4_F \times 24_P$	2.000000000000	2.470471774947
$4_F \times 28_P$	2.000000000000	2.474474352391
$4_F \times 32_P$	2.000000000000	2.477235439183
$4_F \times 36_P$	2.000000000000	2.479250359727
$4_F \times 40_P$	2.000000000000	2.480784447068
$5_F \times 5_P$	2	
$5_F \times 10_P$	2.000000004274	2.485912024903
$5_F \times 15_P$	2	
$5_F \times 20_P$	2.000000000000	2.546528797961
$5_F \times 25_P$	2	
$5_F \times 30_P$	2.000000000000	2.560437990844
$5_F \times 35_P$	2	
$5_F \times 40_P$	2.000000000000	2.566264491529
$5_F \times 45_P$	2	
$5_F \times 50_P$	2.000000000000	2.569485040710
$6_F \times 6_P$	2.000004484676	2.407498857052
$6_F \times 12_P$	2.000000000000	2.559303044172
$6_F \times 18_P$	2.000000000000	2.591819531465
$6_F \times 24_P$	2.000000000000	2.604283491675
$6_F \times 30_P$	2.000000000000	2.610364438319
$6_F \times 36_P$	2.000000000000	2.613696502926
$6_F \times 42_P$	2.000000000000	2.615612713769
$6_F \times 48_P$	2.000000000000	2.616718339556
$6_F \times 54_P$	2.000000000000	2.617340472059
$6_F \times 60_P$	2.000000000000	2.617677872418
$7_F \times 7_P$	2	
Beraha	2	2.618033988750

Table 5: Real zeros of the chromatic polynomial $P_{m\times n}(q)$ of a square-lattice strip of width m and lengths $n = k \times m$ $(k = 1, \ldots, 10)$ with cyclic boundary conditions. A blank means that the zero in question is absent. The first two real zeros $q = 0, 1$ are exact on all lattices. For $m = 2$ we have only found these two first zeros. "Beraha" indicates the Beraha numbers $B_4 = 2$ and $B_5 = (3 + \sqrt{5})/2$.

Lattice	4th Zero	5th Zero	6th Zero	7th Zero
$2_F \times 2_P$	3			
$2_F \times 4_P$	2.515844688131	3	3.408771911807	
$2_F \times 6_P$	2.640265063616			
$2_F \times 8_P$	2.616262917475	2.751508037623	3	
$2_F \times 10_P$	2.614657987429	3	3.138323546170	
$2_F \times 12_P$	2.621439264722			
$2_F \times 14_P$	2.616560224418	2.887655738411	3	
$2_F \times 16_P$	2.618700179921	3	3.083264711515	
$2_F \times 18_P$	2.617797220618			
$2_F \times 20_P$	2.618107109614	2.926805351303	3	
$3_F \times 3_P$	2.546602348484			
$3_F \times 6_P$	2.617993627116			
$3_F \times 9_P$	2.618034110186	2.937234729089		
$3_F \times 12_P$	2.618033988011			
$3_F \times 15_P$	2.618033988754	2.965427896259		
$3_F \times 18_P$	2.618033988750			
$3_F \times 21_P$	2.618033988750	2.976132937129		
$3_F \times 24_P$	2.618033988750			
$3_F \times 27_P$	2.618033988750	2.981774802850		
$3_F \times 30_P$	2.618033988750			
$4_F \times 4_P$	2.617986010522	3	3.465246100723	
$4_F \times 8_P$	2.618033988761	3	3.230317951180	
$4_F \times 12_P$	2.618033988750	3.000090191719	3.165028046404	
$4_F \times 16_P$	2.618033988750	3	3.231342732991	
$4_F \times 20_P$	2.618033988750	3	3.219343048602	
$4_F \times 24_P$	2.618033988750	3.000000003255	3.200001385558	
$4_F \times 28_P$	2.618033988750	3	3.219217913659	
$4_F \times 32_P$	2.618033988750	3	3.217140972107	
$4_F \times 36_P$	2.618033988750	3.000000000000	3.210324007476	
$4_F \times 40_P$	2.618033988750	3	3.218488888204	
$5_F \times 5_P$	2.618033990394	3		
$5_F \times 10_P$	2.618033988750	3	3.246585484861	
$5_F \times 15_P$	2.618033988750	2.999999999573	3.250186825428	3.287751313682
$5_F \times 20_P$	2.618033988750	3	3.246967522201	
$5_F \times 25_P$	2.618033988750	3	3.246982088945	3.332102289607
$5_F \times 30_P$	2.618033988750	3.000000000000	3.246977286183	
$5_F \times 35_P$	2.618033988750	3	3.246979668997	3.329353767785
$5_F \times 40_P$	2.618033988750	3	3.246979593498	
$5_F \times 45_P$	2.618033988750	3.000000000000	3.246979607399	3.327447532663
$5_F \times 50_P$	2.618033988750	3	3.246979603508	
$6_F \times 6_P$	2.618033988750	3.001033705947	3.125892136302	
$6_F \times 12_P$	2.618033988750	3.000000000036	3.246874398154	
$6_F \times 18_P$	2.618033988750	3.000000000000	3.246979478144	
$6_F \times 24_P$	2.618033988750	3.000000000000	3.246979603417	
$6_F \times 30_P$	2.618033988750	3.000000000000	3.246979603717	
$6_F \times 36_P$	2.618033988750	3.000000000000	3.246979603717	
$6_F \times 42_P$	2.618033988750	3.000000000000	3.246979603717	
$6_F \times 48_P$	2.618033988750	3.000000000000	3.246979603717	
$6_F \times 54_P$	2.618033988750	3.000000000000	3.246979603717	
$6_F \times 60_P$	2.618033988750	3.000000000000	3.246979603717	
$7_F \times 7_P$	2.618033988750	3	3.247001348628	3.404690481534
Beraha	2.618033988750	3	3.246979603717	3.414213562373

Table 6: Real zeros of the chromatic polynomial $P_{m\times n}(q)$ of a triangular-lattice strip of width m and lengths $n = k \times m$ $(k = 1, \ldots, 10)$ with cyclic boundary conditions. A blank means that the zero in question is absent. The first three real zeros $q = 0, 1, 2$ are exact on all lattices. "Beraha" indicates the Beraha numbers $B_5 = (3+\sqrt{5})/2$, $B_6 = 3$, B_7, and B_8.

	Eigenvalue-Crossing Curves $\mathcal{B}$						Isolated Points
Lattice	# C	# E	# T	# D	# ER	q_0	# RI
2_R	1	0	0	1	2	3	2
3_R	1	0	8	1	6	3	2
4_R	$1^\dagger$	$0^\dagger$	$8^\dagger$	$0^\dagger$	$5^\dagger$	3.2281262261	2
5_R	$1^\dagger$	$0^\dagger$	$16^\dagger$	$0^\dagger$	$9^\dagger$	3.3324469422	3
6_R	$1^\dagger$	$2^\dagger$	$10^\dagger$	$0^\dagger$	$5^\dagger$	3.4062849655	3
7_F	$1^\dagger$	$2^\dagger$	$12^\dagger$	$0^\dagger$	$6^\dagger$	3.4682618071	3
8_F						3.5134782609	3

Table 7: Summary of qualitative results for the triangular-lattice eigenvalue-crossing curves $\mathcal{B}$ and for the isolated limiting points of zeros. For each cyclic triangular-lattice strip considered in this paper, we give the number of connected components of $\mathcal{B}$ (# C), the number of endpoints (# E), the number of T points (# T), the number of double points (# D), and the number of enclosed regions (# ER). We also give the value q_0 which is the largest real value where $\mathcal{B}$ intersects the real axis, and the number of real isolated limiting points of zeros (# RI). The symbol † indicates uncertain results.

q	Lattice	L	ℓ	f
B_5	Square	6	0	0.28823784
		7	0	0.28514284
		8	0	0.28291082
B_5	Triangular	2	1	−0.24060591
		3	0	−0.35114882
		4	1	−0.46727989
		5	0	−0.48121183
		6	1	−0.48248246
		7	0	−0.52290292
		8	1	−0.53899001
B_7	Triangular	5	0	0.11980838
		6	0	0.11458681
		7	0	0.11124861
		8	0	0.10886700

Table 8: Real free energy for $q = B_n$ with integer n. For several values of $q = B_n$ we list the free energy associated to the most relevant eigenvalue of the transfer matrix that gives a non-zero contribution to the partition function. For each value of q, the type and width L of the lattice strip, we list the sector ℓ the eigenvalue belongs to and the free energy f.

m	SqRing	SqRingT	# blocks	max dim	SqRing$'$
2	4	4	3	2	4
3	20	15	4	7	10
4	94	60	5	25	26
5	614	342	6	127	70

Table 9: Block structure of the square-lattice transfer matrix acting on the top and bottom rows $\widehat{\mathsf{T}}$ (A.2). For each strip width m, we quote the dimension of the standard connectivity-state basis $\{\boldsymbol{w}\}$ SqRing and the dimension of the t-reflection-invariant basis SqRingT. We also give the number of blocks (# blocks) the transfer matrix $\widehat{\mathsf{T}}$ can be decomposed, the dimension of the largest block (max dim), and the number of distinct eigenvalues we find SqRing$'$.

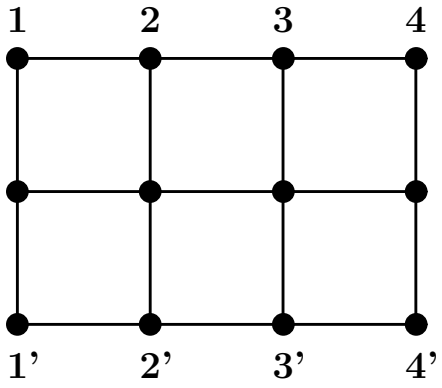

Figure 1: Square lattice with cyclic boundary conditions of size 4×2. This lattice is obtained from a square lattice with free boundary conditions of size 4×3 by identifying the top and bottom rows $i \leftrightarrow i'$ $(i = 1, \ldots, 4 = m)$.

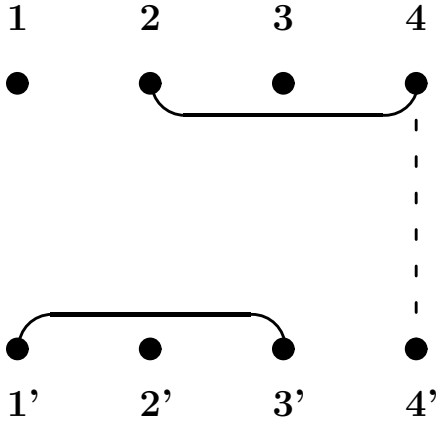

Figure 2: Connectivity state for a cyclic strip of width 4. As an example, we show the connectivity state $\mathcal{P} = \delta_{1',3'}\delta_{2,4,4'}$. This state can be seen as a bottom-row connectivity state $\mathcal{P}_{\text{bottom}} = \delta_{1',3'}$ (solid line), a top-row connectivity state $\mathcal{P}_{\text{top}} = \delta_{2,4}$ (solid line), and a bridge connecting both rows $\delta_{4,4'}$ (dashed line).

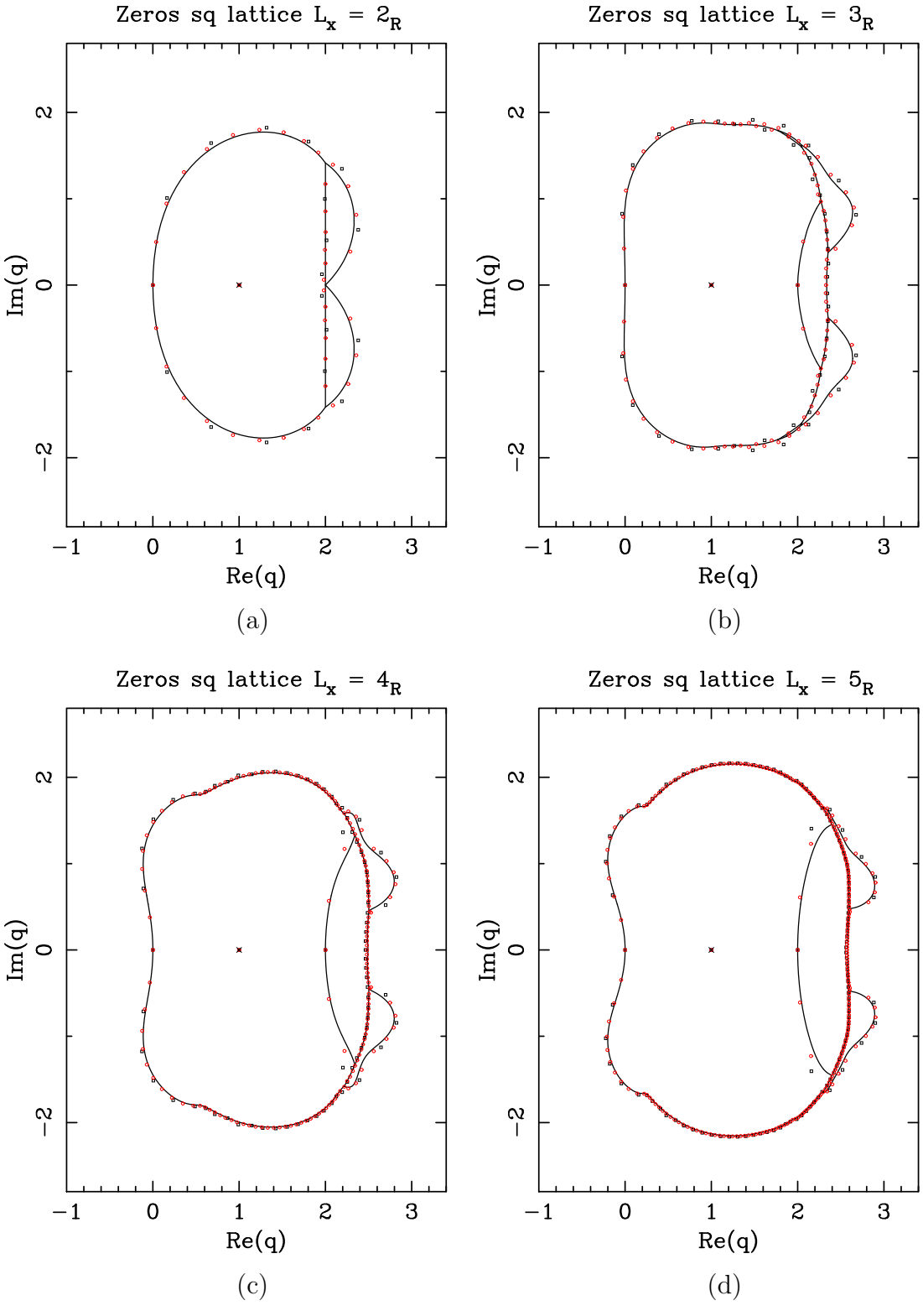

Figure 3: Limiting curves for square-lattice strips of width (a) $L = 2$, (b) $L = 3$, (c) $L = 4$, and (d) $L = 5$ with cyclic boundary conditions. We also show the zeros for the strips $L_{\rm F} \times (5L)_{\rm P}$ (black $\square$) and $L_{\rm F} \times (10L)_{\rm P}$ (red $\circ$) for the same values of L.

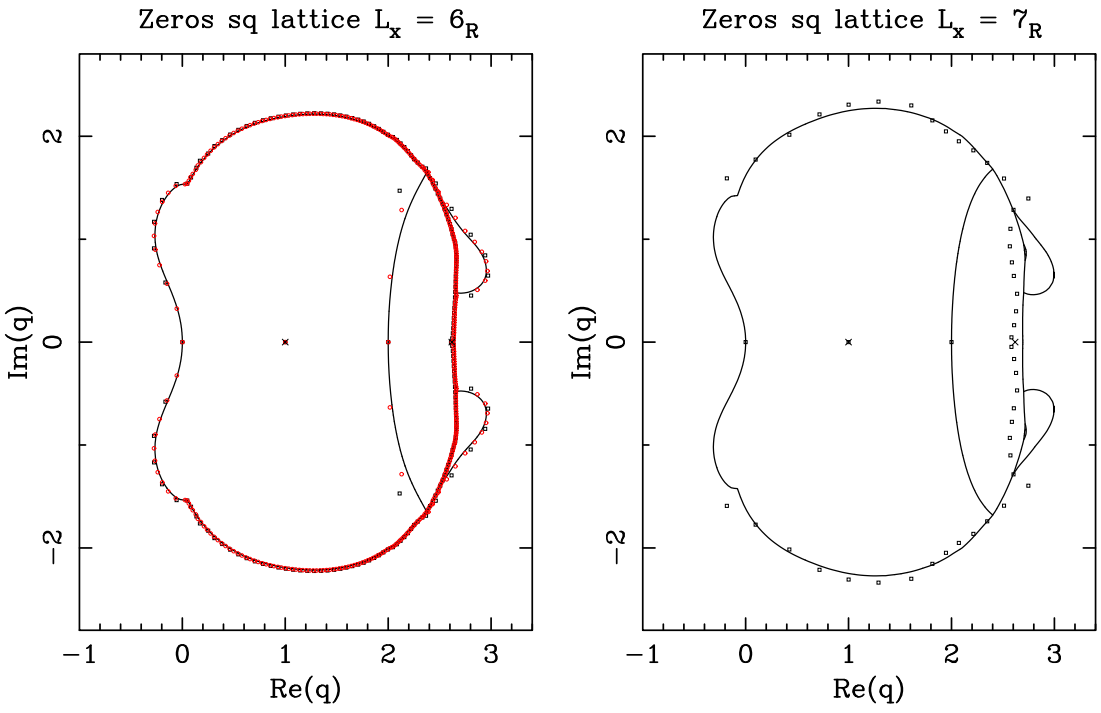

Figure 4: Limiting curves for square-lattice strips of width (a) $L = 6$, and (b) $L = 7$ with cyclic boundary conditions. In (a) we show the zeros for the strips $6_F \times 30_P$ (black $\square$) and $6_F \times 60_P$ (red $\circ$). In (b) we show the chromatic zeros for the strip $7_F \times 7_P$ (black $\square$).

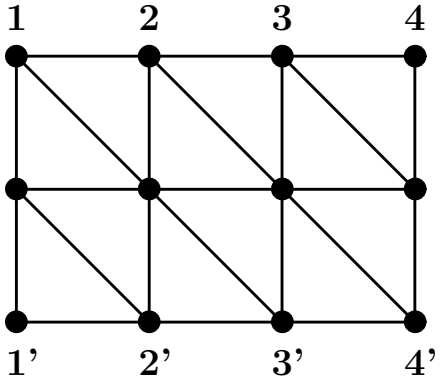

Figure 5: Triangular lattice with cyclic boundary conditions of size 4×2. This lattice is obtained from a triangular lattice with free boundary conditions of size 4×3 by identifying the top and bottom rows $i \leftrightarrow i'$ $(i = 1, \ldots, 4)$.

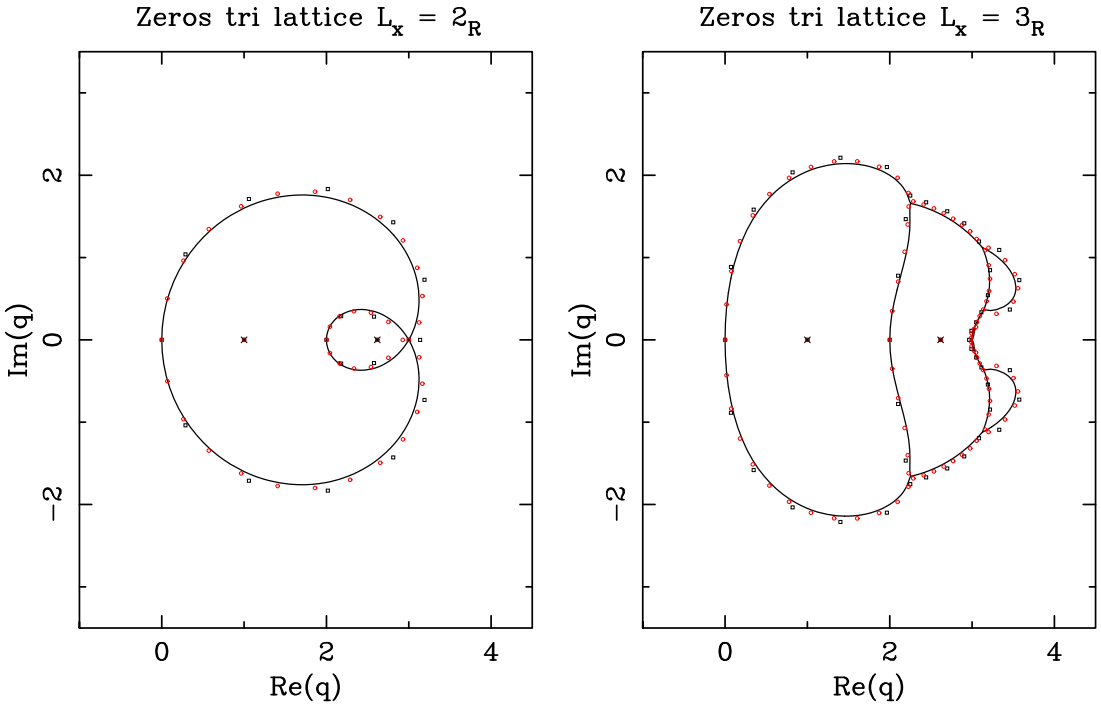

(a)

(b)

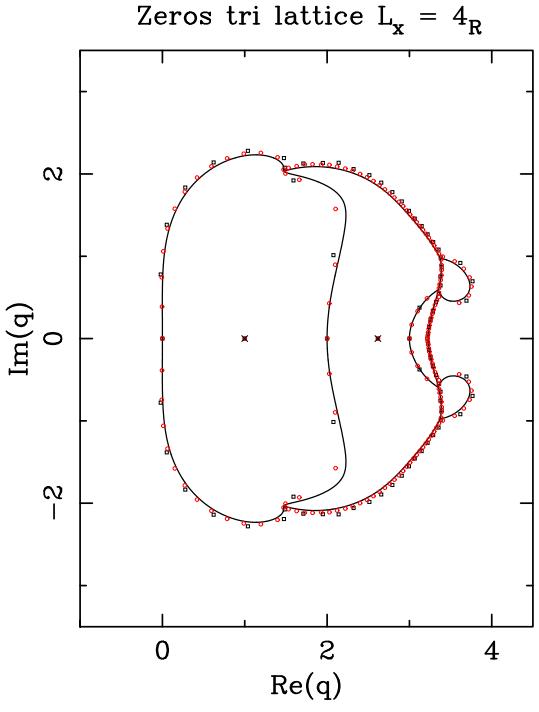

(c)

Figure 6: Limiting curves for triangular-lattice strips of width (a) $L = 2$, (b) $L = 3$, and (c) $L = 4$ with cyclic boundary conditions. We also show the zeros for the strips $L_{\rm F} \times (5L)_{\rm P}$ (black $\square$) and $L_{\rm F} \times (10L)_{\rm P}$ (red $\circ$) for the same values of L.

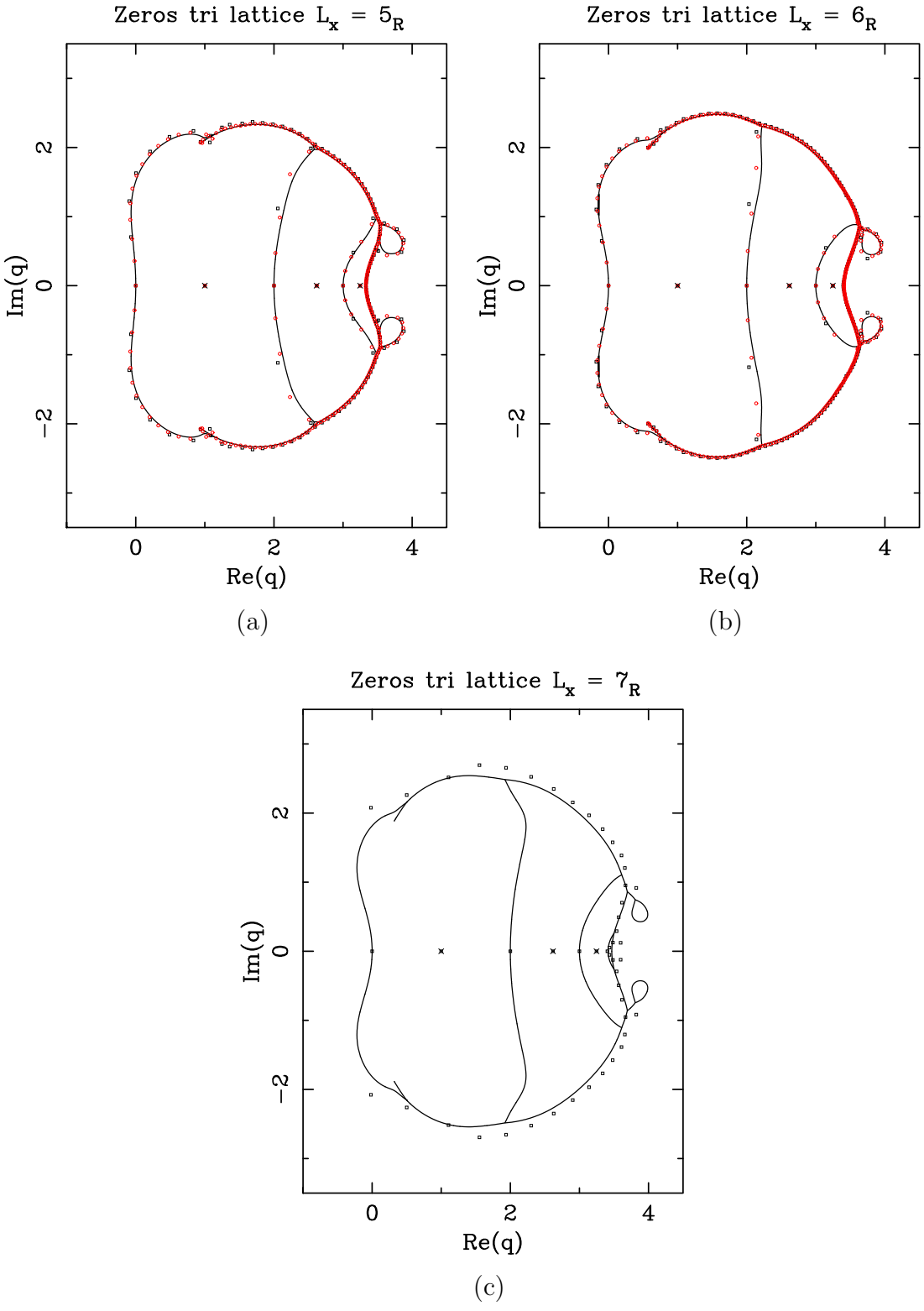

Figure 7: Limiting curves for triangular-lattice strips of width (a) $L = 5$, (b) $L = 6$, and (c) $L = 7$ with cyclic boundary conditions. We also show the zeros for the strips $L_{\rm F} \times (5L)_{\rm P}$ (black $\Box$) and $L_{\rm F} \times (10L)_{\rm P}$ (red $\circ$) for $L = 4, 5$. For $L = 7$ we show the chromatic zeros for the strip $7_{\rm F} \times 7_{\rm P}$ (black $\Box$).

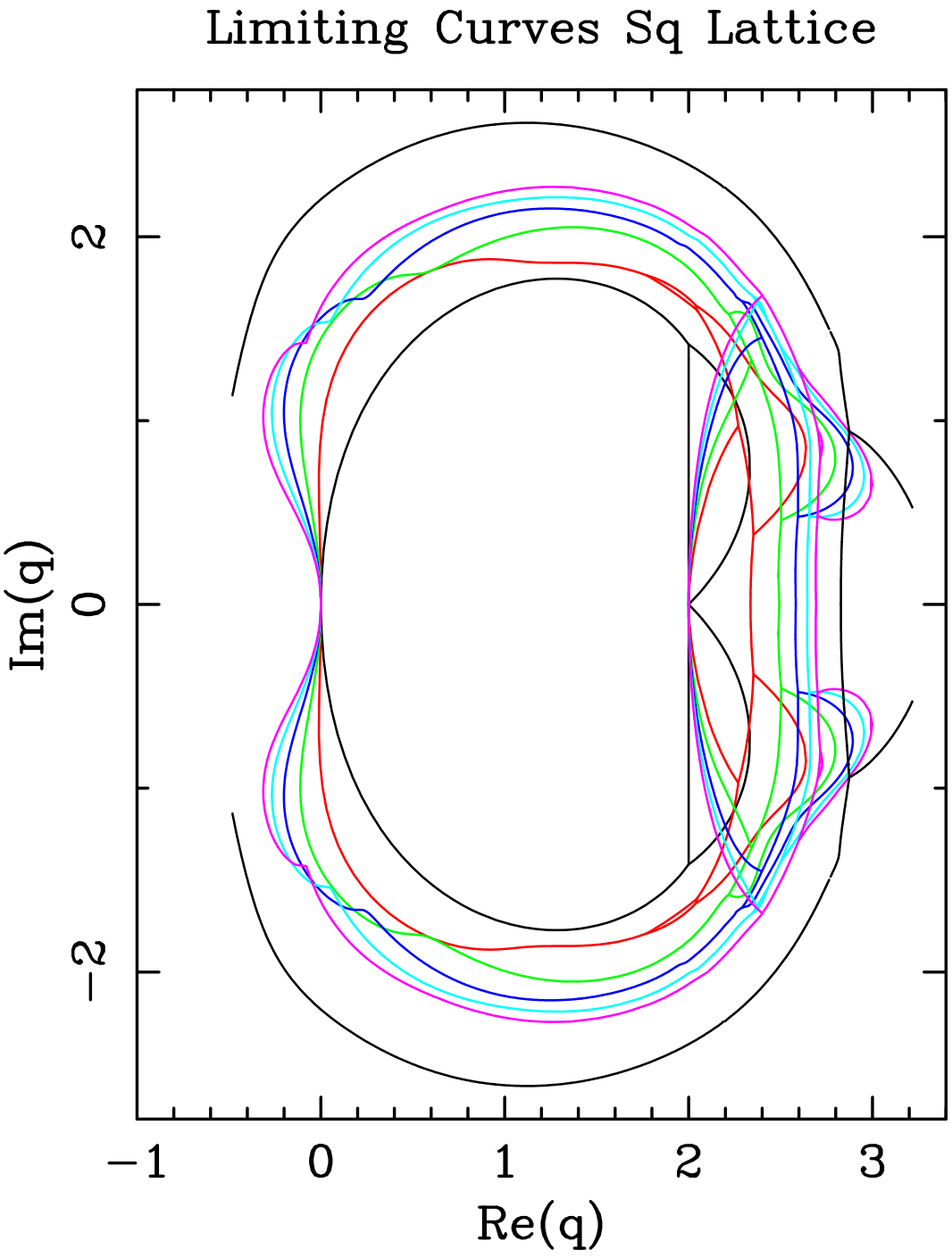

Figure 8: Limiting curves for square-lattice strips of width L and cyclic boundary conditions. We show the results for $L = 2$ (black), $L = 3$ (red), $L = 4$ (green), $L = 5$ (blue), $L = 6$ (light blue), and $L = 7$ (pink). The outermost (black) curve shows the limiting curve for a square-lattice strip of width $L = 10$ with cylindrical boundary conditions [23].

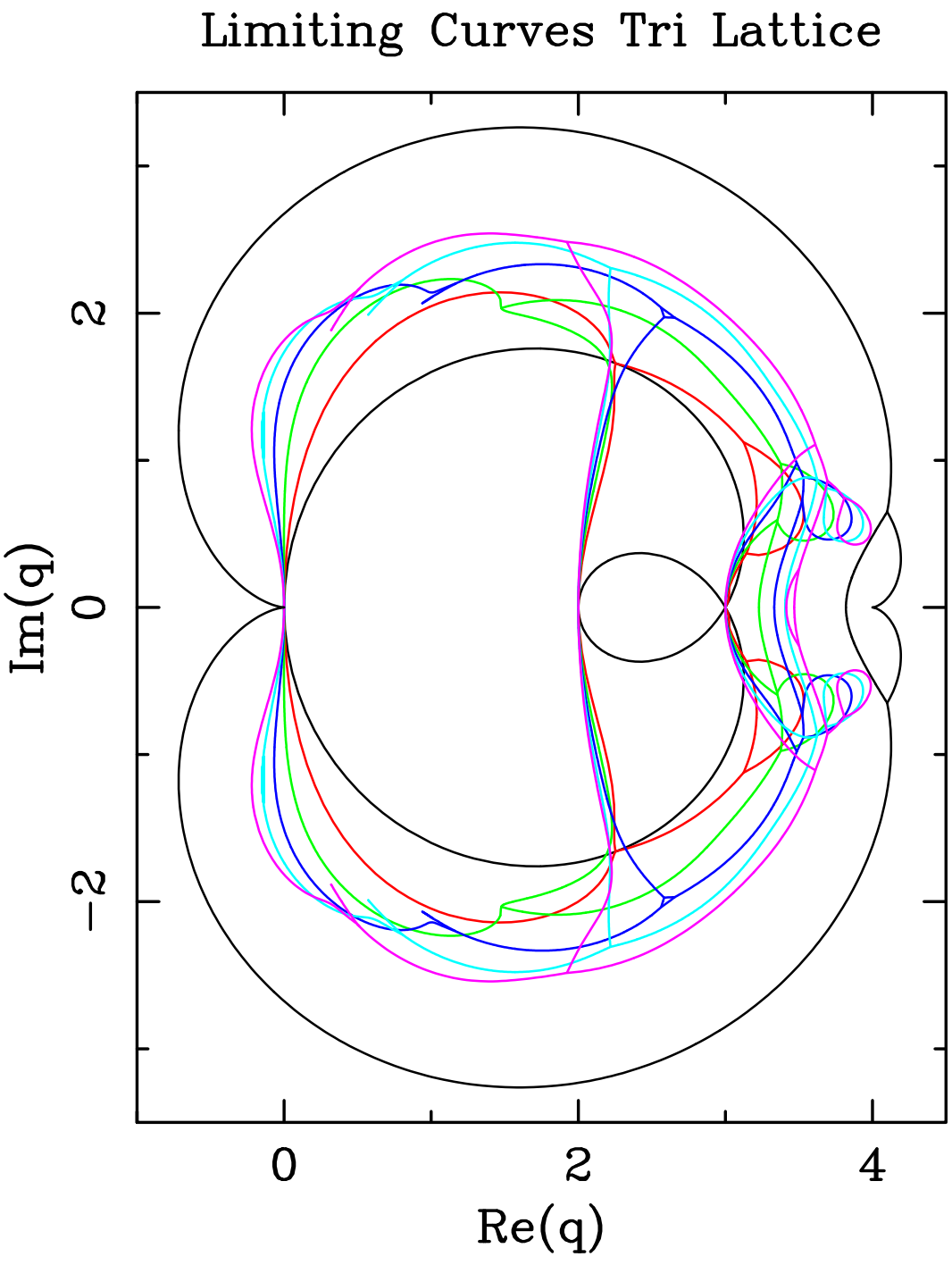

Figure 9: Limiting curves for triangular-lattice strips of width L and cyclic boundary conditions. We show the results for $L = 2$ (black), $L = 3$ (red), $L = 4$ (green), $L = 5$ (blue), and $L = 6$ (light blue), and $L = 7$ (pink). The outermost (black) curve shows the infinite-volume limiting curve obtained by Baxter [21]. See [24] for a critical discussion on Baxter's limiting curve.

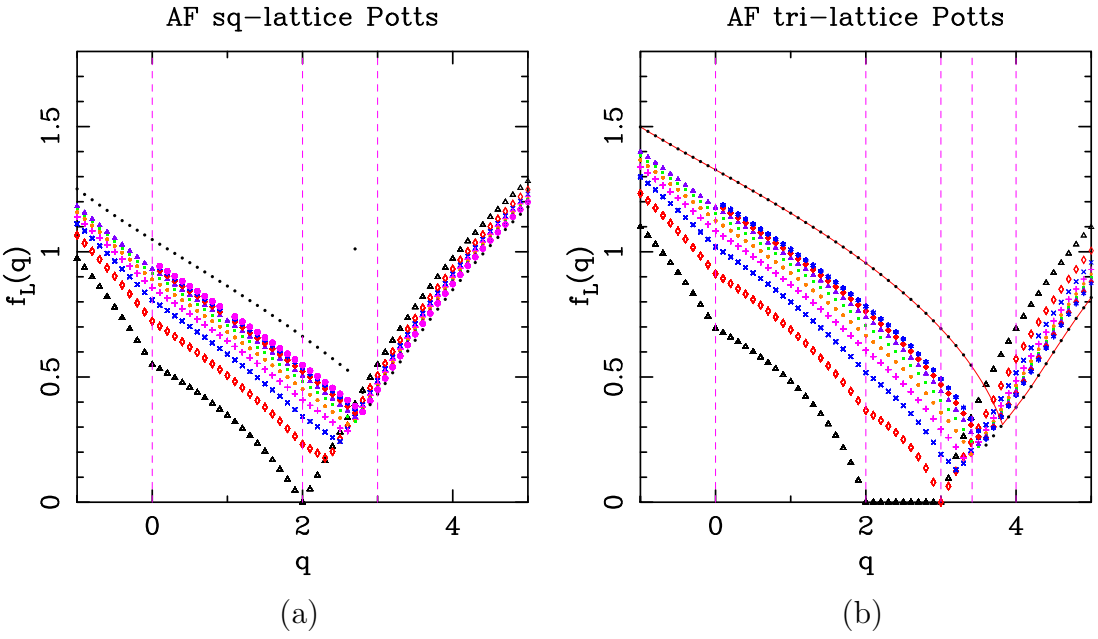

(a) (b)

Figure 10: Estimates of the free energy for the square- (a) and triangular-lattice (b) Potts model for real q in the range $-1 \le q \le 5$. In each plot we show the values of the free energy obtained from the leading eigenvalue of the transfer matrix for strip widths $L = 2$ (black $\triangle$), 3 (red $\diamond$), 4 (blue $\times$), 5 (pink $+$), 6 (orange $\bullet$), 7 (green $\blacksquare$), 8 (violet $\blacktriangle$), 9 (red $\blacklozenge$), 10 (blue $*$), and 11 (pink $\oplus$). We also show the extrapolated value of the free energy in the thermodynamic limit (black $\bullet$) obtained by performing the fit (6.3) for $L_{\min} = 7$ (resp. $L_{\min} = 6$) for the square (resp. triangular) lattice. In (b) the solid (red) line shows the exact value of the triangular-lattice free energy found by Baxter [21]. The vertical (pink) dashed lines show even Beraha numbers $q = B_{2n} = B_{2n}^{(1)}$ (2.29). In (a) we show $1 \le n \le 3$, and in (b), $1 \le n \le 4$ and the limit $n \to \infty$ (i.e., $q = 4$).

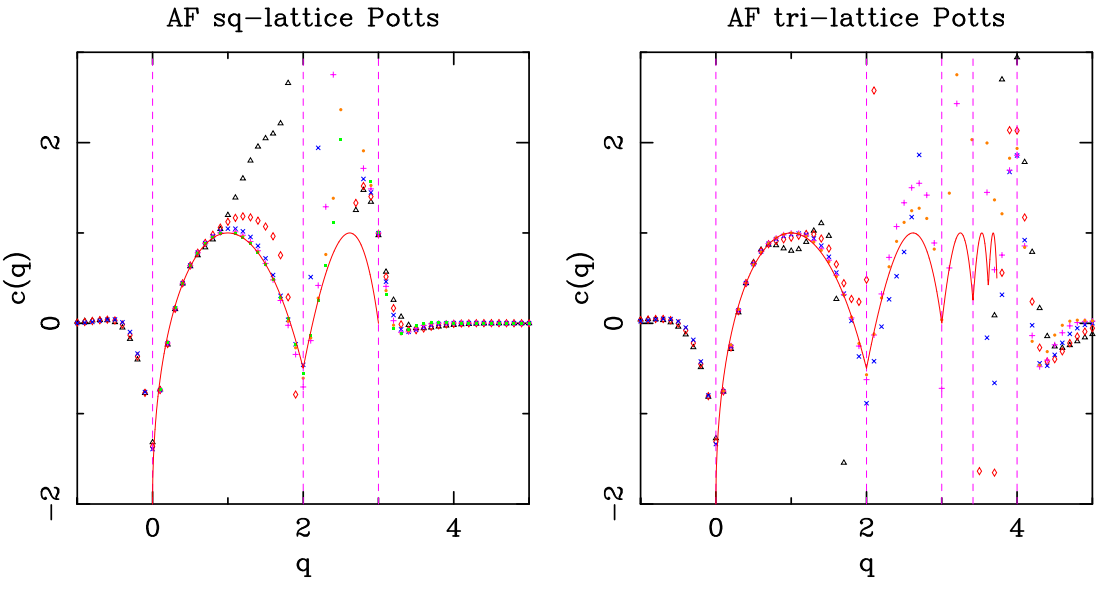

Figure 11: Estimates of the central charge for the zero-temperature Potts antiferromagnet on the square (a) and triangular (b) lattices for real q in the range $-1 \le q \le 5$. In each plot we show the values of the central charge obtained from the fits to the Ansatz (6.3) for $L_{\min} = 2$ (black $\triangle$), 3 (red $\diamond$), 4 (blue $\times$), 5 (pink $+$), 6 (orange $\bullet$), and 7 (green $\blacksquare$). The solid (red) line shows the theoretical prediction for the effective central charge $c_{\rm eff}$ (6.6). The vertical (pink) dashed lines are as in Figure 10.

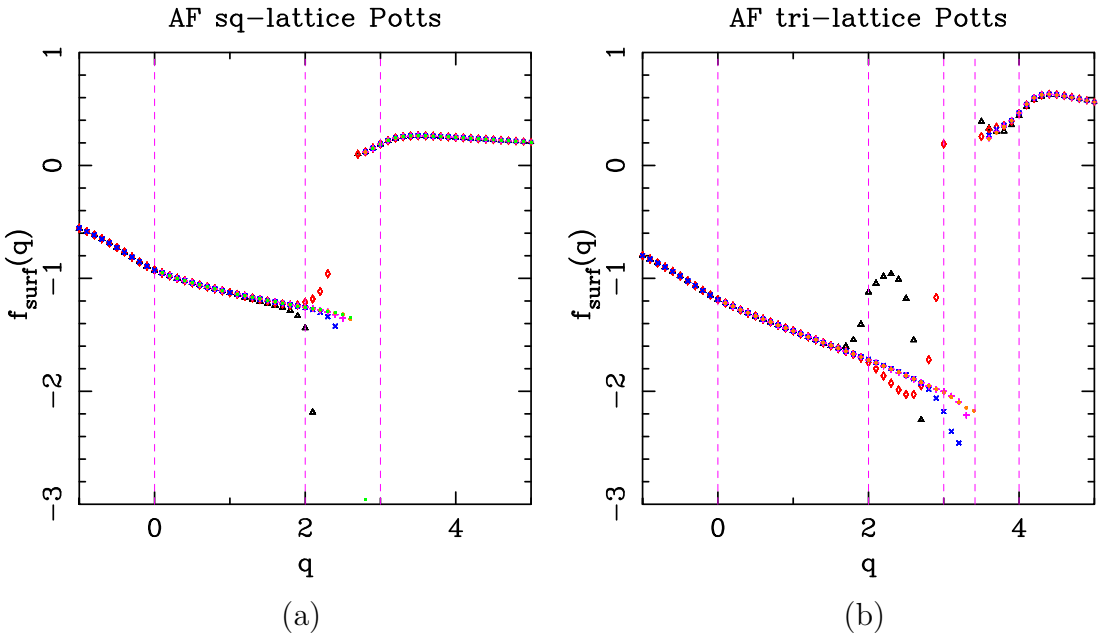

(a) (b)

Figure 12: Estimates of the surface free energy $f_{\rm surf}(q)$ for the zero-temperature Potts antiferromagnet on the square (a) and triangular (b) lattices for real q in the range $-1 \le q \le 5$. In each plot we show the values of the surface free energy obtained from the fits to the Ansatz (6.3) for $L_{\min} = 2$ (black $\triangle$), 3 (red $\diamond$), 4 (blue $\times$), 5 (pink $+$), 6 (orange $\bullet$), and 7 (green $\blacksquare$). The vertical (pink) dashed lines are as in Figure 10.

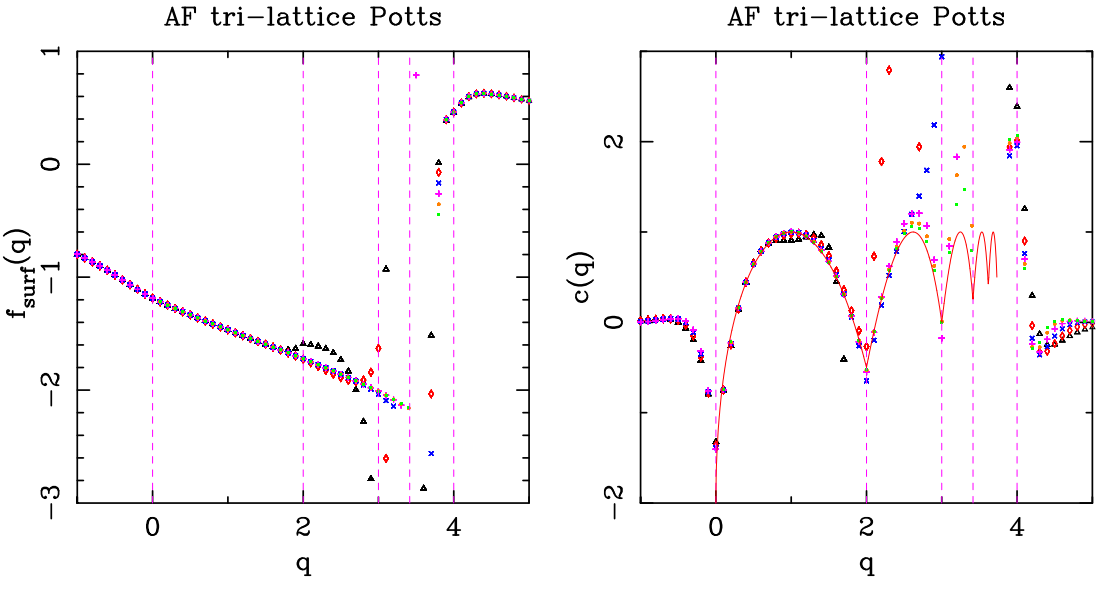

(a) (b)

Figure 13: Estimates of the surface free energy $f_{\rm surf}(q)$ (a) and the central charge $c(q)$ (b) on the triangular lattice when $f_{\rm bulk}(q)$ in the Ansatz (6.3) is fixed to its analytically known value [21]. We show the estimates of $f_{\rm surf}(q)$ and $c(q)$ for real q in the range $-1 \le q \le 5$ and different values of $L_{\rm min} = 2$ (black $\triangle$), 3 (red $\diamond$), 4 (blue $\times$), 5 (pink $+$), 6 (orange $\bullet$), and 7 (green $\blacksquare$). The solid (red) line in (b) shows the theoretical prediction for the effective central charge $c_{\rm eff}$ (6.6). The vertical (pink) dashed lines are as in Figure 10.